J Physiol 602.20 (2024) pp 5179–5201

The Journal of Physiology

Dual ablation of the RyR2-Ser2808 and RyR2-Ser2814 sites increases propensity for pro-arrhythmic spontaneous Ca^{2+} releases

Radoslav Janicek[1], Emmanuel M. Camors[2], Duilio M. Potenza[1], Miguel Fernandez-Tenorio[1], Yanting Zhao[3], Holly C. Dooge[3], Randall Loaiza[3], Francisco J. Alvarado[3], Marcel Egger[1], Hector H. Valdivia[3] and Ernst Niggli[1]

[1]*Department of Physiology, University of Bern, Bern, Switzerland*
[2]*Department of Pediatrics, Division of Cardiology, University of Tennessee Health Science CenterLe Bonheur Children's Hospital Research Center, Memphis, TN, USA*
[3]*Cardiovascular Research Center, University of Wisconsin-Madison School of Medicine and Public Health, Madison, WI, USA*

Handling Editors: Bjorn Knollmann & Eleonora Grandi

The peer review history is available in the Supporting Information section of this article (https://doi.org/10.1113/JP286453#support-information-section).

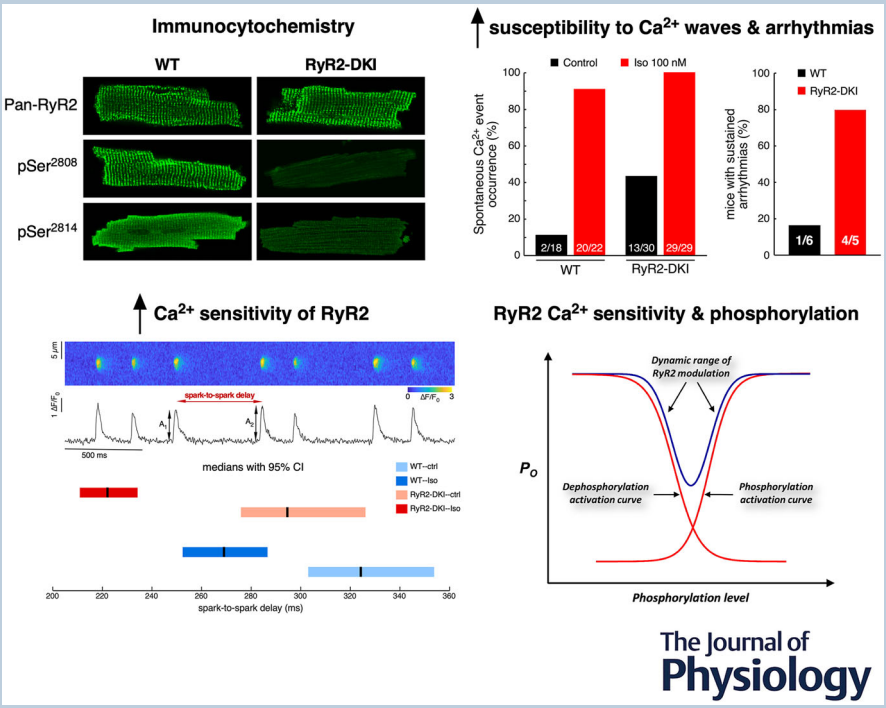

Abstract figure legend Immunocytochemistry reveals the ablation of ryanodine receptor (RyR2)-S2808 and S-2814 phosphorylation sites in cardiac myocytes from transgenic mice. This leads to increased susceptibility to Ca^{2+} waves and arrhythmias in double-knock-in (RyR-DKI) compared to wild-type (WT) mice. Spark recovery kinetics are accelerated in control conditions and in the presence of isoprenaline (Iso), suggesting elevated Ca^{2+} sensitivity of the RyRs harbouring the mutations. A simple model implementing an increase of the open probability (P_o) for both RyR2 hyper- and hypophosphorylation can explain our findings.

R. Janicek and E. M. Camors contributed equally to this work.

DOI: 10.1113/JP286453

Abstract During exercise or stress, the sympathetic system stimulates cardiac contractility via β-adrenergic receptor (β-AR) activation, resulting in phosphorylation of the cardiac ryanodine receptor (RyR2). Three RyR2 phosphorylation sites have taken prominence in excitation–contraction coupling: S2808 and S2030 are described as protein kinase A specific and S2814 as a Ca^{2+}/calmodulin kinase type-2-specific site. To examine the contribution of these phosphosites to Ca^{2+} signalling, we generated double knock-in (DKI) mice in which Ser2808 and Ser2814 phosphorylation sites have both been replaced by alanine (RyR2-S2808A/S2814A). These mice did not exhibit an overt phenotype. Heart morphology and haemodynamic parameters were not altered. However, they had a higher susceptibility to arrhythmias. We performed confocal Ca^{2+} imaging and electrophysiology experiments. Isoprenaline was used to stimulate β-ARs. Measurements of Ca^{2+} waves and latencies in myocytes revealed an increased propensity for spontaneous Ca^{2+} releases in DKI myocytes, both in control conditions and during β-AR stimulation. In DKI cells, waves were initiated from a lower threshold concentration of Ca^{2+} inside the sarcoplasmic reticulum, suggesting higher Ca^{2+} sensitivity of the RyRs. The refractoriness of Ca^{2+} spark triggering depends on the Ca^{2+} sensitivity of the RyR2. We found that RyR2-S2808A/S2814A channels were more Ca^{2+} sensitive in control conditions. Isoprenaline further shortened RyR refractoriness in DKI cardiomyocytes. Together, our results suggest that ablation of both the RyR2-Ser2808 and RyR2-S2814 sites increases the propensity for pro-arrhythmic spontaneous Ca^{2+} releases, as previously suggested for hyperphosphorylated RyRs. Given that the DKI cells present a full response to isoprenaline, the data suggest that phosphorylation of Ser2030 might be sufficient for β-AR-mediated sensitization of RyRs.

(Received 20 March 2024; accepted after revision 21 August 2024; first published online 23 September 2024)
Corresponding authors E. Niggli, Department of Physiology, University of Bern, CH-3012 Bern, Switzerland. Email: ernst.niggli@unibe.ch and H. H. Valdivia, University of Wisconsin, Cardiovascular Research Center, Madison WI, 53705, U.S.A. Email: hvaldivia@wisc.edu

Key points

- Phosphorylation of cardiac sarcoplasmic reticulum Ca^{2+}-release channels (ryanodine receptors, RyRs) is involved in the regulation of cardiac function.
- Ablation of both the RyR2-Ser2808 and RyR2-Ser2814 sites increases the propensity for pro-arrhythmic spontaneous Ca^{2+} releases, as previously suggested for hyperphosphorylated RyRs.
- The intra-sarcoplasmic reticulum Ca^{2+} threshold for spontaneous Ca^{2+} wave generation is lower in RyR2-double-knock-in cells.
- The RyR2 from double-knock-in cells exhibits increased Ca^{2+} sensitivity.
- Phosphorylation of Ser2808 and Ser2814 might be important for basal activity of the channel.
- Phosphorylation of Ser2030 might be sufficient for a β-adrenergic response.

Introduction

In cardiac muscle, the ryanodine receptors (RyR2) govern Ca^{2+} release from the sarcoplasmic reticulum (SR), thereby regulating cardiac contractile force. These intracellular membrane channels are activated with every heartbeat via the Ca^{2+}-induced Ca^{2+} release mechanism (for a review, see Bers, 2002). During each systole, the RyR2s generate a large number of synchronized elementary SR Ca^{2+} events, Ca^{2+} sparks. Ca^{2+}-induced Ca^{2+} release is normally triggered by Ca^{2+} entering via L-type Ca^{2+} channels, but RyR2s can also give rise to potentially arrhythmogenic spontaneous Ca^{2+} release events during diastole, such as spontaneous Ca^{2+} sparks or Ca^{2+} waves.

During the last few years, it has become evident that RyR2s are subject to regulation by post-translational protein modifications (for a review, see Niggli et al., 2013). Notably, a substantial body of literature addresses the role of RyR2 phosphorylation. RyR2 phosphorylation is extensively regulated by the adrenergic system, for example, during stress or the 'fight-or-flight' response.

In addition, many cardiac diseases, such as heart failure, impact on or remodel the associated cellular signalling pathways. On the RyR2, three phosphorylation sites and their associated protein kinases have gained prominence because of their apparent functional relevance. These are the serine residues 2808 and 2814 (rabbit nomenclature used throughout) in the 'phosphorylation hotspot' (Haji-Ghassemi et al., 2019; Valdivia, 2012) and the more recently characterized serine 2030 (Potenza et al., 2019; Wei et al., 2023; Xiao et al., 2005). Details of the functional consequences of RyR2 phosphorylation, such as the role of the various sites and the involved protein kinases [e.g. protein kinase A (PKA) and Ca^{2+}/calmodulin kinase type-2 (CaMKII)] are still not completely settled, yielding apparently conflicting results. An overriding consensus, however, is that phosphorylation of RyR2 generally intensifies RyR2 channel activity and Ca^{2+} sensitivity, whereas RyR2 dephosphorylation opposes or reduces these effects (Terentyev & Hamilton, 2016).

The estimated extent of constitutive phosphorylation in control conditions, frequently determined with phospho- or dephosphoepitope-specific antibodies, varies between the three sites, being highest at Ser2808 (George, 2008; Huke & Bers, 2008). *In vivo*, the steady-state extent of phosphorylation for each site will depend not only on the activity of the protein kinases, but also on the balanced activity of protein phosphatases. Of note, phosphatases PP1 and PP2B are anchored to the RyR2 macromolecular complex and might thereby have preferential access to specific RyR2 phospho-sites.

In this context, the functional consequences of RyR2 dephosphorylation have so far received less attention than those related to RyR2 phosphorylation or its presumed pathological excess, loosely termed 'hyper-phosphorylation' (Marx et al., 2000). Nonetheless, there are several publications in which acute dephosphorylation of the RyR2 has been investigated using phosphatases, mostly in experiments with RyR2s reconstituted into lipid bilayers or with the analysis of Ca^{2+} sparks in permeabilized single cardiomyocytes (e.g. see Lokuta et al., 1995; Potenza et al., 2020; Terentyev & Hamilton, 2016; Terentyev et al., 2003). Furthermore, several transgenic animal models have been engineered to examine constitutive phosphorylation of the various sites (e.g. the phospho-mimetic RyR2-S2808D and RyR2-S2814D knock-in mice). As negative controls, RyR2-S2808A and RyR2-S2814A mice, in which the RyRs are constitutively dephosphorylated and cannot be phosphorylated, were also examined (reviewed by Dobrev & Wehrens, 2014; Houser, 2010). From these studies, the emergent general picture was that phosphorylation, particularly of the Ser2814 site, leads to higher RyR2 activity, whereas constitutively dephosphorylated RyR2 channels generally appear to restrain the function of RyR2s.

In the present study, we examined a unique mouse line with constitutive ablation of both the Ser2808 and the Ser2814 phospho-sites [RyR2-S2808A/S2814A double knock-in (DKI) mice]. Therefore, among the three most prominent phospho-sites, only serine 2030 remained available for regulation by phosphorylation. Surprisingly, cardiomyocytes harbouring the DKI RyR2s presented with an elevated susceptibility to arrhythmogenic Ca^{2+} waves and a higher Ca^{2+} spark frequency upon β-adrenergic stimulation in comparison to cells from wild-type (WT) animals. This was paralleled by a reduced Ca^{2+} concentration and lower Ca^{2+} wave threshold inside the SR. Spark recovery analysis suggested a higher Ca^{2+} sensitivity of the DKI RyR2s in control conditions. Interestingly, upon β-adrenergic stimulation, these channels still exhibited an increase of their Ca^{2+} sensitivity, possibly mediated by phosphorylation of the remaining RyR2-Ser2030 site and, potentially, other phospho-sites not yet identified. Taken together, these findings suggest a complex and non-linear interaction between the various phosphorylation sites on the RyR2s.

Methods

Ethical approval

Housing and breeding of the mice was carried out in the departmental animal facility, with free access to rodent laboratory chow and water. All mice were handled with permission of the State Veterinary Administration and according to Swiss Federal Animal Protection law (permit BE 6/19) and the Institutional Animal Care and Use

Radoslav Janicek received his PhD in animal physiology from the Comenius University in Bratislava. After a postdoctoral stay at Rutgers New Jersey Medical School in Newark, he moved to Bern, to the Department of Physiology of the University of Bern. His research focuses on calcium signalling in cardiac myocytes, using a combination of confocal imaging, electrophysiological techniques and photolysis of caged compounds. **Emmanuel M. Camors** received his PhD in cardiac physiology from the University of Denis Diderot in Paris. After two postdoctoral fellowships, at the University of California in Davis and the University of Michigan in Ann Arbor, he joined the Department of Pediatrics at the University of Tennessee Health Science Center in Memphis to develop a translational research laboratory focusing on inherited cardiomyopathies. Using a combination of fluorescence and confocal microscopy, surface ECG assessments, histological staining and molecular biology assays, his group studies the molecular determinants of arrhythmogenic cardiomyopathy.

Committee (IACUC) of the University of Wisconsin, and all the experiments were carried out in accordance with the approved guidelines and the policy and regulations on animal experimentation of *The Journal of Physiology* (Grundy, 2015). In this study, we used both female ($N = 35$) and male ($N = 47$) mice.

Generation of the RyR2-S2808A/S2814A (DKI) mouse

A portion of 8 kb of *Ryr2* containing exon 57 was obtained by screening the 129Sv CITB BAC library (Invitrogen, Carlsbad, CA, USA) and subcloned into pBluescript KS vector upstream from a MC1-HSV-TK cassette. A FRT-Puro-FRT selection cassette was introduced by recombineering downstream of exon 57. The TCT > GCG mutation (Ser > Ala) was introduced into exon 57 by PCR using the following primer: 5′-TCAATCACCAGGTCGCGATAGAT-3′. A NruI restriction site was introduced to identify the mutant allele (Ala2814). NotI linearized targeting vector was electroporated into mouse R1 embryonic stem cells containing the homozygote Ryr2-Ser2808ala mutation (Benkusky et al., 2007). Homologous recombinants were selected for growth on puromycin and G418. Screening of the clones by Southern blot identified one clone carrying the mutations RyR2-Ser2808Ala/Neomycin and RyR2-Ser2814/Puro on the same chromosome. The karyotypically normal targeted clone was next injected into a C57Bl/6 blastocyst at the university of Yale. Two chimeric founders were then backcrossed ≥10 times with 129S1/SvlmJ partners (#002448, The Jackson Laboratory) to create a genetically pure 129/Sv-RyR2-DKI mouse line. Mice carrying the mutations RyR2-Ser2808Ala/Ser2814Ala were identified by PCR according to Benkusky et al. (2007).

Isolation of ventricular cardiomyocytes

Ventricular myocytes were isolated from homozygous RyR2-S2808A$^{+/+}$/S2814A$^{+/+}$ (RyR2-DKI) (Camors, Loaiza, et al., 2012, Camors et al., 2014; Mondragón et al., 2014) and WT littermates following an established protocol (Louch et al., 2011; Zhao et al., 2015). Adult mice were killed by cervical dislocation, and the hearts were excised, cannulated and retrogradely perfused on a Langendorff system. Hearts were perfused at 37°C for ∼15 min with a Ca^{2+}-free modified Tyrode solution composed of (in mmol/l): 140 NaCl, 5.4 KCl, 1.1 $MgCl_2$, 10 Hepes, 1 NaH_2PO_4 and 10 glucose (pH 7.4). Cells were enzymatically dissociated using a cocktail of collagenase type II (160 U/ml; Worthington) and/or protease type XIV (0.21 U/ml; Sigma). After isolation, ventricular myocytes were kept at room temperature in a modified Tyrode solution containing 1.0 or 1.8 mmol/l $CaCl_2$ and used within 6 h.

Echocardiography and ECG assessments

Echocardiography was performed on 3-month-old mice ($N = 13$ per group). Animals were anaesthetized in an induction chamber by 5% isoflurane mixed with 0.8–1 l/min oxygen and maintained in an anaesthetized state by 1−2% isoflurane. Mice were then placed in a supine position atop a heating pad with ECG leads. Their body temperature was monitored continuously and maintained at 37 ± 0.2°C throughout the recordings. Transthoracic echocardiography was performed using a 22−55 MHz probe (MS550D) connected to a Vevo 2100 system (Visual Sonic, Toronto, ON, Canada). Cardiac assessments were obtained and analysed by an operator blinded to the mouse groups using VevoLab 2.1 software (Visual Sonic). Surface ECGs were recorded in slightly anaesthetized (1–2% isoflurane) mice ($N = 6$ or 7 mice per group) on a heated pad in a supine position. Needle ECG electrodes were placed under the skin in an equivalent of the lead II configuration. Baseline ECGs were recorded for 5 min, followed by intraperitoneal injection of an adrenaline (2 mg/kg body weight) and caffeine (120 mg/kg body weight) cocktail to activate the sympathetic pathway. Mouse ECGs were recorded for an additional 30 min. ECG signals were recorded using an Octal Bio Amplifier connected to a Powerlab 8/35 (ADInstruments, Colorado Springs, CO, USA) and analysed by a blinded operator using LabChart 7.0 software (ADInstruments). Mean ECG values were calculated as the average of four sets of 10 consecutive beats. Arrhythmic events were segregated by duration between non-sustained (≤5 s) and sustained (>5 s) arrhythmias.

Ex vivo heart performance

After cervical dislocation, the heart of adult mice ($N = 6$ WT and 5 RyR2-DKI) was excised and quickly cannulated by the aorta to a Langendorff perfusion apparatus (ADInstruments). Hearts were perfused at 2–2.5 ml/min with a heated (37°C) and oxygenated Krebs–Henseleit buffer containing (in mmol/l): 118.5 NaCl, 4.7 KCl, 1.2 $MgSO_4$, 1.2 KH_2PO_4, 11 glucose, 25 $NaHCO_3$ and 1.8 $CaCl_2$. A pressure transducer continuously recorded the left ventricular developed pressure via a water-filled balloon inserted into the left ventricular chamber by the mitral valve after excision of the left atria. Following a 30 min stabilization period, a β-adrenergic response was elicited by the perfusion of 200 nmol/l isoprenaline (Iso) and recorded for an extra 5 min. Then, explanted hearts were quickly frozen in liquid N_2 and stored at −80°C for further analysis. The left

ventricular pressures were recorded and analysed using LabChart6 software (ADInstruments). Exclusion criteria included hearts exhibiting a basal diastolic pressure of >10 mmHg or a systolic pressure of <80 mmHg.

Excitation–contraction coupling gain recordings

Excitation–contraction coupling gain was measured by simultaneous recording of the L-type Ca^{2+} channel current and the resulting Ca^{2+} transient in isolated myocytes. Whole-cell patch clamp was performed by using an Axopatch 200B amplifier and a Digitdata 1322A digitizer (Molecular Devices, San Jose, CA, USA). The Ca^{2+} current was recorded at room temperature in cells perfused by 1.8 mmol/l $CaCl_2$ Tyrode solution plus 30 µmol/l tetrodotoxin (Na^+ channel blocker) and 10 mmol/l 4-aminopyridine. The pipette internal solution contained (in mmol/l): 110 CsCl, 6 $MgCl_2$, 5 Na_2ATP, 0.3 Na_2GTP, 10 Hepes, 15 tetraethylammonium chloride and 10 µmol/l Fluo-4 pentapotassium salt, pH 7.2 (adjusted with CsOH). Cells were voltage clamped at −70 mV, then depolarized from −60 to +70 mV in 10 mV increments for 300 ms and repolarized to −70 mV between sweeps. The resulting Ca^{2+} transients were recorded simultaneously by laser scanning confocal microscopy using a LSM 510-META microscope (Carl Zeiss USA, White Plains, NY, USA) with a C-Apochromat ×40 water-immersion objective lens (n.a. = 1.2). Myocytes were loaded for 30 min (at room temperature) with 10 µmol/l of the Fluo-4 AM dye in 1 mmol/l $CaCl_2$ Tyrode solution plus 0.005% pluronic acid (Invitrogen). The complete de-esterification of the dye occurred during a 30 min wash (Camors, Mohler, et al., 2012). Isoprenaline (100 nmol/l) was used to activate the β-adrenergic response (Benkusky et al., 2007). Fluo-4 was excited at 488 nm by an argon laser, and the fluorescent signal was collected through a 505 nm long-pass emission filter. The Ca^{2+} transients were recorded in line-scan mode at 330 Hz along the length of the myocytes. The SR Ca^{2+} load was estimated by the rapid application of 10 mmol/l caffeine. Fluorescence data were analysed using ImageJ software (NIH).

Ca^{2+} transients and Ca^{2+} wave latency

Adult ventricular myocytes were loaded for 30 min at room temperature with the Ca^{2+}-sensitive fluorescent dye Fluo-3 AM (5 µmol/l; Biotium, Fremont, CA, USA). After 30 min perfusion to allow for de-esterification with modified Tyrode solution (in mmol/l: 140 NaCl, 5.4 KCl, 1.8 $CaCl_2$, 1.1 $MgCl_2$, 10 Hepes, 1 NaH_2PO_4 and 10 glucose; pH 7.4) myocytes were paced at 1 Hz for 30 s. Ca^{2+} signals were recorded by confocal microscopy (Olympus FluoView 1200; ×60 water immersion objective) in line-scan mode. Fluo-3 was exited at 488 nm with a solid-state laser (Coherent, Santa Clara, CA, USA), and light emission was acquired at a wavelength of >500 nm. A line-scan image lasting ∼50 s was acquired before and 3 min after application of 100 nmol/l Iso (Camors, Mohler, et al., 2012). Rapid application of caffeine (4 s, 10 mmol/l) was used to assess SR Ca^{2+} content. Line-scan images were analysed using a custom-written program in MATLAB. Spontaneous Ca^{2+} signalling events were analysed within a 30 s interval after the beginning of the last triggered transient. Wave amplitudes and decay time constants were calculated from deskewed Ca^{2+} waves. Caffeine-induced Ca^{2+} transients were not considered for the analysis of SR Ca^{2+} content if a spontaneous Ca^{2+} wave occurred within the preceding 3 s. Box-and-whisker plots with overlying scatter plots were used to show the distributions of the measured parameters of Ca^{2+} signals. Each circle represents a measurement from an individual cell.

Recording of Ca^{2+} sparks in intact myocytes

Isolated cardiomyocytes were loaded for 30 min (at room temperature) in 1 mmol/l $CaCl_2$ Tyrode solution with the intracellular Ca^{2+} dye Fluo-4 AM (10 µmol/l) plus 0.005% pluronic acid (Invitrogen). After a 30 min wash, myocytes were paced at 1 Hz in 1.8 mmol/l $CaCl_2$ Tyrode solution. At the steady state (2 min), the pacing was stopped, and Ca^{2+} sparks were recorded for 14 s. Sparks were detected using line-scan microscopy (LSM510-META, Carl Zeiss USA) with a plan-apochromat ×60 oil objective (n.a. = 1.4). The pixel size was set at 0.14 µm, and the recording was done at 520 Hz. The SR Ca^{2+} load was determined by a 10 mmol/l caffeine application. Ca^{2+} spark characteristics were analysed using homemade routines in IDL (Harris Geospatial, Broomfield, CO, USA). The mass of Ca^{2+} sparks was calculated according to Hollingworth et al. (2001) as Ca^{2+} sparks amplitude × 1.206 × (full width at half maximum)^3, and the RyR2-mediated leak as Ca^{2+} sparks mass × Ca^{2+} sparks frequency.

Recording of Ca^{2+} sparks in permeabilized myocytes

Spontaneous Ca^{2+} sparks were recorded in cells permeabilized by exposure to β-escin for 60 s (in mmol/l: 100 potassium aspartate, 20 KCl, 3.7 $MgCl_2$, 0.5 EGTA, 10 Hepes and 0.005% β-escin; pH 7.2). Permeabilized ventricular myocytes were then resuspended in an escin-free solution adjusted for detection of Ca^{2+} sparks (in mmol/l: 120 potassium aspartate, 3 K_2ATP, 0.5 EGTA, 3 $MgCl_2$, 10 phosphocreatine, 5 U/ml creatine phosphokinase, 50 µmol/l Fluo-3-K_5 salt, 50 nmol/l free Ca^{2+}; pH 7.2). Free Ca^{2+} concentrations were measured and corrected using a NanoDrop ND-3300 (Thermo Fisher Scientific, Basel, Switzerland) fluorospectrometer and the Indo-1-K_5 salt Ca^{2+} indicator (10 µmol/l;

Biotium). Ca^{2+} sparks were recorded with a confocal microscope (Olympus FluoView 1000; ×60 water immersion objective) operating in line-scan mode at a rate of ∼ 500 lines/s. Fluo-3 (Biotium) was exited at 473 nm with a solid-state laser (MLL-FN-473, Changchun New Industries Optoelectronics Technology Co., China), and light emission was acquired at wavelengths of >500 nm. Ca^{2+} sparks in permeabilized myocytes were recorded in control conditions and after treatment with PP1 catalytic subunit (PP1c; 2 U/ml for 1−5 min) or cAMP (5 µmol/l). SR Ca^{2+} content was assessed using rapid caffeine exposure (20 mmol/l). Line-scan images were analysed using a custom program written in MATLAB. An approach developed by Bankhead et al. (2011) was applied to detect Ca^{2+} sparks. Data were visualized as box-and-whisker plots with an overlying scatter plot, where each circle represents an individual cell.

Sarcoplasmic reticulum Ca^{2+} measurements

Fluo-5N AM (Thermo Fisher Scientific, USA) and rhod-2-K_3 (Teflabs, Austin, TX, USA,) salt were used to measure SR and cytosolic Ca^{2+} changes, respectively (Fernandez-Tenorio & Niggli, 2016). The SR of isolated cardiomyocytes was loaded with 12.5 µmol/l of the Ca^{2+}-sensitive dye Fluo-5N AM for 3 h at 37°C. Subsequently, cells were permeabilized irreversibly by exposure to saponin for 45 s (in mmol/l: 100 potassium aspartate, 20 KCl, 3.7 $MgCl_2$, 1 EGTA, 10 Hepes and 0.005% saponin; pH 7.2). Rhod-2-K_3 salt (25 µmol/l) was added to the internal solution (in mmol/l: 120 potassium aspartate, 3 K_2ATP, 0.1 EGTA, 3 $MgCl_2$, 0.012 $CaCl_2$, 10 phosphocreatine, 5 U/ml creatine phosphokinase and 10 Hepes; free intracellular Ca^{2+} was set to 100 nmol/l; pH 7.2). Free Ca^{2+} concentrations were measured and corrected as described above. Blebbistatin (25 µmol/l) was used to avoid sarcomere contractions. The images were acquired with a confocal microscope in the line-scan mode. Line-scan images were analysed in ImageJ using custom-written macros.

Ca^{2+} spark recovery analysis

Isolated cardiac myocytes were loaded with Fluo-3 AM (5 µmol/l; Biotium) and EGTA AM (5 µmol/l; AAT Bioquest, Pleasanton, CA, USA) for 30 min at room temperature, followed by 30 min de-esterification. They were placed in a recording chamber with an experimental solution containing (in mmol/l): 140 NaCl, 1.1 $MgCl_2$, 5.4 KCl, 1 NaH_2PO_4, 10 Hepes, 10 glucose and 1 $CaCl_2$; pH 7.4. A low dose of ryanodine (50 nmol/l; Alomone Labs, Jerusalem, Israel) was used to evoke repetitive Ca^{2+} sparks as previously described (Sobie et al., 2005). A fresh aliquot of ryanodine was used for each experimental day. Ryanodine exposure was limited in time to avoid of appearance of long-lasting Ca^{2+} sparks. Before recording, cells in the Iso experimental group were exposed to 100 nmol/l Iso for 3 min. An experimental solution containing 100 nmol/l Iso and 50 nmol/l ryanodine was subsequently applied to these cells. Ca^{2+} sparks were recorded using Fluo-3 excited at 488 nm with a solid-state laser (Coherent), and fluorescence was recorded at >500 nm. Repetitively firing clusters were identified and scanned with a confocal microscope (Olympus FluoView 1200; ×60 water immersion objective) operated in line-scan mode.

The analysis of the line-scan recordings was performed by a custom program written in MATLAB. The same criteria for selection were applied as in the study by Potenza et al. (2019). Briefly, cells with Ca^{2+} spark frequencies of >15/100 µm/s or cells with long-lasting sparks (>200 ms) were excluded. Moreover, signals with two subpopulations of events (in terms of amplitudes of releases) were excluded because they might reflect the overlap of two clusters of RyR2. A bootstrapping approach was adopted to calculate 95% confidence intervals (CIs) for the spark-to-spark delay medians (Poláková et al., 2015).

Immunostaining

After their isolation, ventricular myocytes were plated on laminin-coated coverslips and fixed in 4% paraformaldehyde (in PBS, pH 7.4). Then, cells were solubilized by 0.1% Triton X-100 and blocked in 2% bovine serum albumin, 0.02% NaN_3 and 2% goat serum. Myocytes were probed with the primary antibodies pan-RyR2 (1:200; MA3-925, ThermoFisher), pSer2808-RyR2 (1:100; custom-made) and pSer2814-RyR2 (1:200; A010-31, Badrilla), followed by goat anti-mouse, Alexa Fluor 488 (1:5000; A-10680, Invitrogen) or goat anti-rabbit, Alexa Fluor 488 (1:5000; A-11008, Invitrogen) secondary antibodies. Individual optical sections of RyR2 staining were obtained by laser-scanning confocal microscopy (LSM510-META, Carl Zeiss USA) using a C-apochromat ×40 water immersion objective lens (n.a. = 1.2). Alexa Fluor probes were excited at 488 nm by an argon laser, and their emission signal was collected through a 505 nm long-pass filter. Fluorescence images were analysed using ImageJ software (NIH).

Western blots

Tissue homogenates from WT and RyR2-DKI mouse hearts were prepared using a homogenization buffer (0.9% NaCl, 10 mmol/l Tris–HCl, pH 6.8) supplemented with 20 mmol/l NaF and protease inhibitors (2 µmol/l leupeptin, 100 µmol/l phenylmethylsulphonyl fluoride, 500 µmol/l benzamidine and 100 nmol/l aprotinin).

After the mechanical homogenization, samples were centrifuged at 1000*g* for 5 min (4°C), and the supernatants were stored at −80°C until use. Protein concentrations were determined using the Bradford method (Bio-Rad).

Fifty micrograms of protein from tissue homogenates was treated with PKA or CaMKII reaction buffers to induce phosphorylation of RyR2. The PKA reaction buffer contained 2 mmol/l $MgCl_2$, 60 mmol/l KCl, 30 mmol/l Hepes pH 7.4, 1 mmol/l EGTA-Na, 20 mmol/l NaF, 2 µmol/l leupeptin, 100 µmol/l phenylmethylsulphonyl fluoride, 500 µmol/l benzamidine, 100 nmol/l aprotinin, 20 mmol/l NaF, 5 µmol/l okadaic acid potassium, 10 U/µl of the catalytic subunit of PKA (539576, Millipore) and 1 mmol/l K_2ATP. The CaMKII reaction buffer contained 2 mmol/l $MgCl_2$, 60 mmol/l KCl, 30 mmol/l Hepes pH 7.4, 10 µmol/l $CaCl_2$, 20 mmol/l NaF, 2 µmol/l leupeptin, 100 µmol/l phenylmethylsulphonyl fluoride, 500 µmol/l benzamidine, 100 nmol/l aprotinin, 20 mmol/l NaF, 5 µmol/l okadaic acid potassium, 1 µl of recombinant CaMKIIδ (PV3373, ThermoFisher), 3 µmol/l CaM (208694, Sigma) and 1 mmol/l K_2ATP. Control reactions were carried out in PKA reaction buffer without the addition of the enzyme.

For western blotting, samples were separated by a 4−20% SDS-PAGE gradient gel (Bio-Rad), then transferred onto a PVDF membrane using the iblot-2 system (ThermoFisher). Membranes were probed with the following primary antibodies using the ibind flex system (ThermoFisher): anti-RyR [clone 34C] (1:2000; MA3-925, ThermoFisher), pS2808-RyR (1:1000, custom-made; Benkusky et al., 2007), pS2030 (1:1000, custom-made; Zheng et al., 2022), pS2814 (1:2000, A010-31, Badrilla), SERCA1/2 (1:2000; A010-21, Badrilla), pan-PLB (1:5000; MA3-922, TermoFisher), pSer16-PLB (1:5000; A010-12, Badrilla) and pThr17-PLB (1:5000; A010-13, Badrilla) (Benkusky et al., 2007; Camors et al., 2022; Zheng et al., 2022). Secondary antibodies, used as appropriate, were goat anti-mouse-HRP (1:1000 or 1:5000; 31437, ThermoFisher) or goat anti-rabbit-HRP (1:1000 or 1:5000; 31463, ThermoFisher). Membranes were developed using SuperSignal ECL reagent (ThermoFisher) and imaged with a ChemiDoc MP apparatus (Bio-Rad). Band intensity was quantified with ImageLab software (Bio-Rad).

All experiments were performed at room temperature (∼22°C), if not stated otherwise. Chemicals were purchased from Sigma–Aldrich unless stated otherwise. Significant statistical differences ($P < 0.05$) are shown as: * *vs*. control and † *vs*. WT. The letter *N* corresponds to the number of animals and the letter *n* to a number of cells. If not stated otherwise in the figure legend, statistical analysis was performed by fitting a generalized linear mixed-effects model with one (animal) or two (animal and cell) levels to data (Sikkel et al., 2017). A pairwise comparison with Benjamini–Hochberg correction was used to test significant differences among individual groups. All statistical analyses were done in MATLAB (Mathworks, USA).

Results

Characterization of the transgenic animals

We have created a novel knock-in mouse model carrying the dual phospho-site ablation RyR2-S2808A and S2814A from our previously studied RyR2-S2808A mouse model (Fig. 1*A*; Benkusky et al., 2007; Potenza et al., 2020). Heterozygous and homozygous RyR2-DKI mice were viable and exhibited a normal lifespan for ≤2 years. Here, we studied 3- to 4-month-old homozygous animals.

To validate our model, we tested RyR2 expression and phosphorylation by western blotting. Figure 1*B* indicates that total RyR2 expression was similar in RyR2-DKI and WT hearts ($P = 0.6439$). Analysis of RyR2-Ser2808 and Ser2814 phosphorylation levels in control conditions confirmed the absence of baseline phosphorylation in the RyR2-DKI hearts (Fig. 1*C*). To test whether the ablation of Ser2808 and Ser2814 phospho-sites impacted Ser2030 phosphorylation, we incubated tissue homogenates in the presence of the catalytic subunit of PKA (cPKA). Figure 1*C* reveals a robust increase of Ser2030 phosphorylation in both WT and RyR2-DKI homogenates. The incubation of protein homogenates with either cPKA or exogenous calmodulin to activate CaMKII to trigger RyR2 phosphorylation in the WT channel confirmed the ablation of Ser2808 and Ser2814 in the RyR2-DKI protein. Finally, immunofluorescence further highlighted the absence of RyR2-Ser2808 and Ser2814 phospho-sites in isolated myocytes (Fig. 1*D*).

Next, we used echocardiographic measurements to assess the cardiac function of RyR2-DKI mice. The RyR2-DKI heart did not show macroscopic structural remodelling. The left ventricular mass to body weight ratio remained within the normal range ($P = 0.5788$; Fig. 1*E*). The ejection fraction of the mutant hearts was also normal ($P = 0.1333$). However, the heart rate of RyR2-DKI mice was higher than the WT (491.49 ± 47.28 and 454.54 ± 30.12 beats/min, respectively, mean ± SD, $P = 0.0138$). All parameters of echocardiographic measurements are summarized in Table 1. Next, we perfused explanted hearts on a Langendorff set-up (Loaiza et al., 2013). We measured no differences in the left ventricular developed pressure of the RyR2-DKI *vs*. WT explanted hearts in baseline conditions and after Iso stimulation (Table 2). This suggested that the adrenergic response of the DKI hearts was not significantly altered.

Excitation–contraction coupling in DKI mice

To define whether the absence of Ser2808 and Ser2814 would lead to a loss of function for the RyR2 and,

thus, modify cardiac myocyte intracellular Ca^{2+} signalling and excitation–contraction coupling (ECC), we recorded simultaneously the current of L-type Ca^{2+} channels and its resulting Ca^{2+} transient by whole-cell patch clamp combined with laser confocal line-scan microscopy in both control and Iso conditions (Zhao et al., 2015). Figure 2*A* shows representative examples of line-scan images with Ca^{2+} currents and Ca^{2+} transients from single cardiac myocyte recordings. In control conditions, Ca^{2+} current densities (in picoamperes per picofarad) were similar between WT and RyR2-DKI cells (Fig. 2*B*; $P = 0.345$). In contrast, the resulting Ca^{2+} transient amplitudes for DKI myocytes were significantly elevated (Fig. 2*C*; $P = 0.0059$). Thus, the ECC gain, defined as the ratio of the Ca^{2+} transient amplitude over its triggering Ca^{2+} current, was also significantly increased in RyR2-DKI myocytes compared with that of WT cells (Fig. 2*D*; $P = 0.0003$). In Iso conditions, the Ca^{2+} current and its resulting Ca^{2+} transient were generally similar in RyR2-DKI myocytes (but larger at positive potentials; Fig. 2*B* and *C*; $P = 0.0009$ and $P = 1.3 \times 10^{-6}$). Thus, the ECC gain was not uniform, resulting in a biphasic curve, with a net decrease at low depolarizing potentials and an increase at potentials of >30 mV. Taken together,

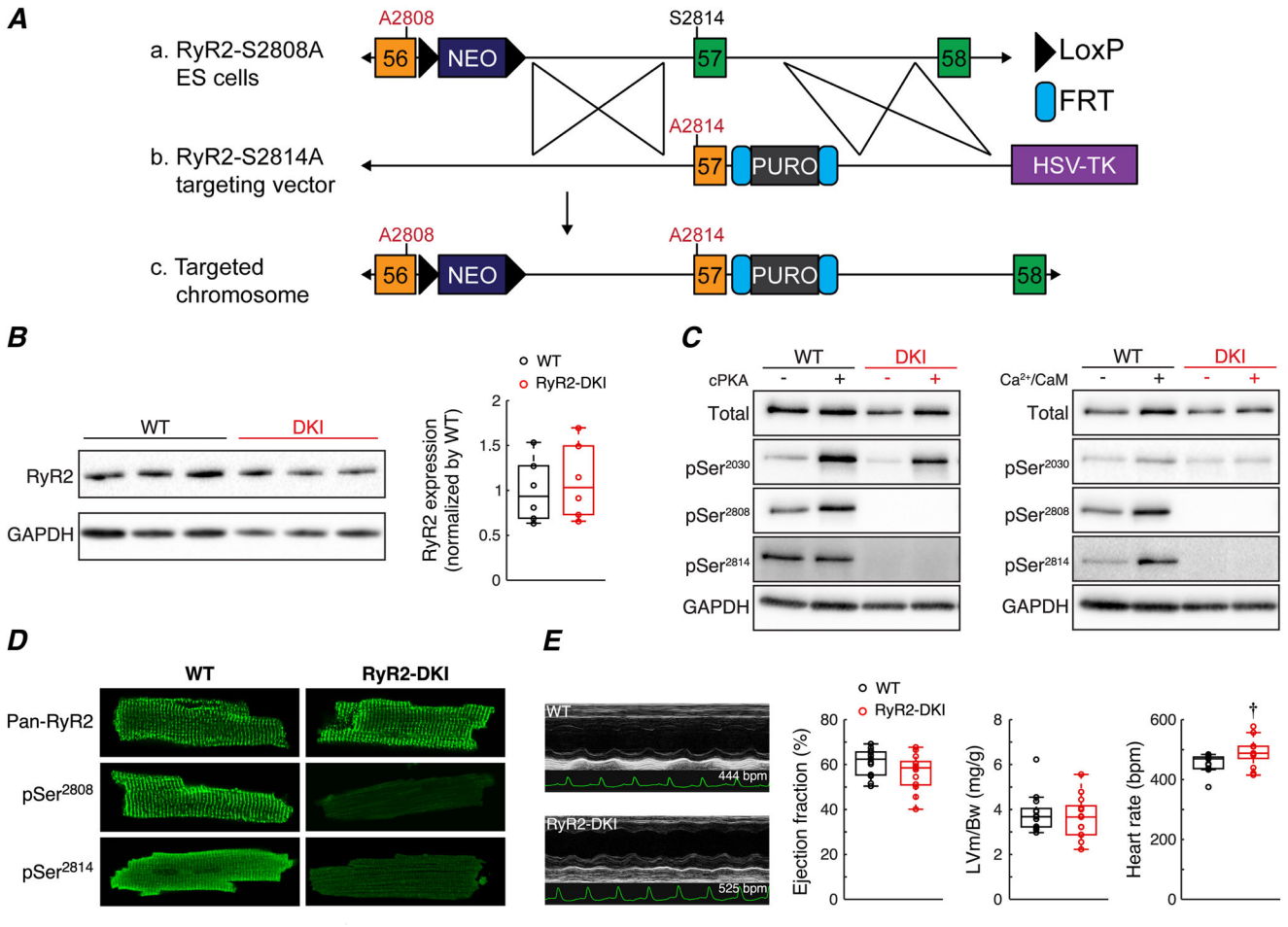

Figure 1. Characterization of double knock-in mice
A, generation of the double knock-in (DKI) mouse line. Please see the Methods section for a complete description. *B*, the total ryanodine receptor (RyR2) expression is comparable in RyR2-DKI and wild-type (WT) animals (Student's two-sample *t* test, $n = 6$, mixed males and females). *C*, western blot analysis confirms the absence of phospho-epitopes Ser2808 and Ser2814 both in control conditions and in the presence of the catalytic subunit of protein kinase A (cPKA) or Ca^{2+}/calmodulin (10 μmol/l Ca^{2+}). A marked increase of Ser2030 phosphorylation after cPKA can be seen in the blots from both animals. *D*, absence of phosphorylation at Ser2808 and Ser2814 confirmed by immunofluorescence in isolated myocytes. *E*, echocardiographic M-mode recording in WT and RyR2-DKI mice. Ventricular mass to body weight ratio and ejection fraction were not significantly different, but the DKI mice exhibited a higher heart rate. $n = 13$ (5 males and 8 females) for WT; $n = 13$ (6 males and 7 females) for RyR2-DKI. Significant differences (†$P < 0.05$ *vs.* WT) were assessed by Student's two-sample *t* test and, in the case of heart rate, by the Wilcoxon rank sum test (to test whether a data sample comes from a normal distribution, the Anderson–Darling test was used).

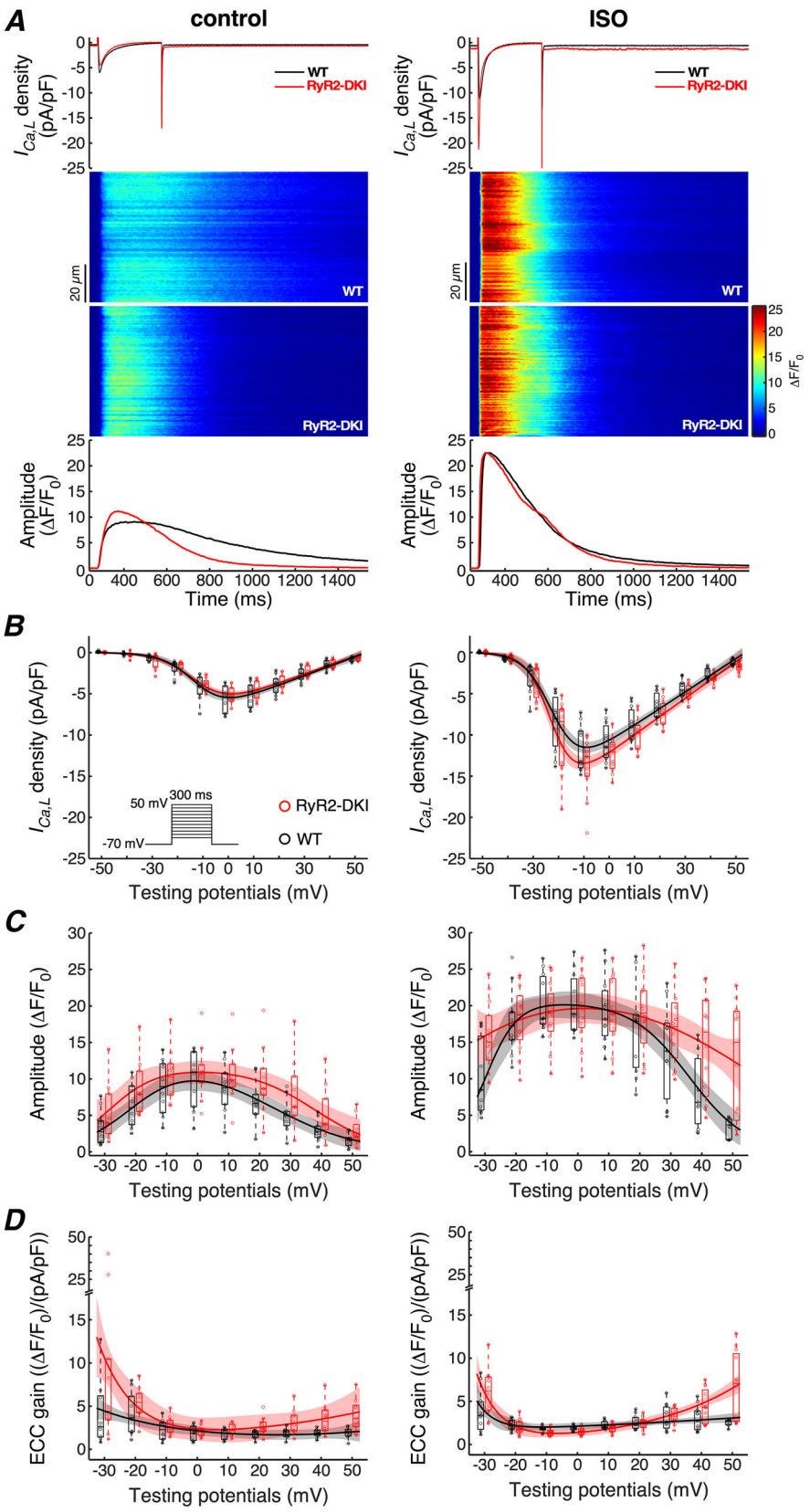

Figure 2. Excitation–contraction coupling in voltage-clamped cardiomyocytes
A, representative example of a voltage-clamped Ca^{2+} transient single cardiac myocyte recording during a voltage step to 0 mV. *B*, current–voltage relationship in control conditions and in the presence of 100 nmol/l isoprenaline

Table 1. M-Mode echocardiography data of wild-type and RyR2-double knock-in mice

Parameter	Units	WT (N = 13)	DKI (N = 13)	P-value
Females		62% (8)	54% (7)	
Heart rate	beats per minute	454.54 ± 30.12	491.49 ± 47.28*	0.0138
LVEDD	millimetres	3.65 ± 0.30	3.72 ± 0.45	0.6356
LVESD	millimetres	2.45 ± 0.36	2.64 ± 0.43	0.2482
LVEDV	microlitres	55.00 ± 11.39	60.74 ± 15.73	0.2976
LVESV	microlitres	21.00 ± 7.27	26.80 ± 10.05	0.1038
FS	percentage	32.03 ± 4.10	29.68 ± 5.42	0.2249
EF	percentage	60.83 ± 6.04	56.50 ± 8.03	0.1333
CO	millilitres per minute	12.60 ± 3.18	15.36 ± 4.91	0.1017
LV mass c	milligrams per gram	3.85 ± 0.85	3.63 ± 0.94	0.5727

Data are shown as the mean ± SD.
* $P < 0.05$ *vs*. WT, assessed by Student's two-sample t test or, in the case of LV mass c and heart rate, by Wilcoxon rank sum test (same as in Fig. 1*E*).
Abbreviations: CO, cardiac output; DKI, double knock-in EF, ejection fraction; FS, fractional shortening; LV mass c, left ventricular mass corrected to body weight; LVEDD/LVESD, left ventricular end-diastolic/end-systolic dimension; LVEDV/LVESV, left ventricular end-diastolic/end-systolic volume; WT, wild type.

Table 2. Langendorff data analysis of left ventricular function of wild-type and double knock-in explanted hearts at baseline and during 200 nmol/l isoprenaline stimulation

Parameter	Units	Baseline		Isoprenaline			
		WT (N = 6)	DKI (N = 5)	WT (N = 6)	P-value	DKI (N = 5)	P-value
Heart rate	beats per minute	385.83 ± 101.57	358.15 ± 57.53	478.94 ± 89.39	0.1304	461.04 ± 40.56*	0.0211
LVEDP	millimetres of mercury	5.82 ± 5.20	3.58 ± 5.86	0.82 ± 10.44	0.2188	−2.22 ± 10.24	0.0625
LVESP	millimetres of mercury	98.31 ± 23.55	98.09 ± 8.96	143.77 ± 20.42*	0.0313	147.75 ± 13.90	0.0625
LVDP	millimetres of mercury	92.49 ± 19.29	94.51 ± 12.30	142.95 ± 24.82*	0.0313	149.98 ± 21.66	0.0625
Con. Vel	10^3 mmHg/s	4.39 ± 1.13	3.91 ± 0.78	9.47 ± 2.32*	0.0011	8.13 ± 1.78*	0.0010
Relax. Vel	-10^3 mmHg/s	2.30 ± 0.40	2.18 ± 0.39	5.72 ± 1.37*	0.0014	5.09 ± 1.00*	0.0015

Data are shown as the mean ± SD. Significant differences were assessed by Student's paired-sample t test (heart rate, Con. Vel and Relax. Vel) or by Wilcoxon signed rank test (LVEDP, LVESP and LVDP).
* $P < 0.05$ *vs*. baseline.
Abbreviations: Con. Vel., contraction velocity; DKI, double knock-in; LVDP, left ventricular developed pressure; LVEDP, left ventricular end-diastolic pressure; LVESP, left ventricular end-systolic pressure; Relax. Vel., relaxation velocity; WT, wild type.

the ECC gain experiments revealed a surprising gain of function for the RyR2 after Ser2808 and Ser2814 ablations.

Next, we tested whether this enhanced RyR2 activity could be reproduced in intact myocytes under 1 Hz field stimulation. In control conditions, we measured comparable amplitudes of Ca^{2+} transients between RyR2-DKI and WT myocytes ($P = 0.5917$; Fig. 3*E*). However, the Ca^{2+} transient decay time was significantly reduced in the RyR2-DKI myocytes compared with that of WT cells (Fig. 3*F*). Nevertheless, at this stimulation frequency the diastolic Ca^{2+} concentration reached immediately before each transient did not differ between WT and DKI cells. Caffeine application revealed comparable SR Ca^{2+} content between both cell types ($P = 0.2010$; Fig. 3*G*). The stimulation of the RyR2-DKI myocytes by Iso highlighted important differences in ECC *vs*. WT cells. Whereas both WT and RyR2-DKI myocytes

(Iso). The voltage-clamp protocol is shown as an inset in the left panel. *C*, the amplitude of the Ca^{2+} transients was comparable, except at very positive voltages, similar to the excitation–contraction coupling (ECC) gain shown in *D*. Data for all parameters at each voltage were tested for outliers using generalized extreme Studentized deviate test for outliers in MATLAB. Box-and-whisker plots with overlying scatter plots were used to show the distributions of the measured parameters of ECC. Each circle represents a measurement from an individual cell. $N = 3–6$, $n = 4–11$ for wild type (WT); $N = 6$, $n = 8–12$ for RyR2-double knock-in (DKI). Continuous lines represent fits with a two-term exponential model (ECC gain), with a Boltzmann function (current–voltage relationship) or with the product of two Boltzmann functions (amplitudes of Ca^{2+} transients). Semi-transparent areas represent 95% confidence intervals for fitted curves. An *F*-test was used to compare global fit (both animal models together) with a sum of separate fits for individual animal models for each parameter–voltage relationship in different experimental conditions.

responded to Iso by increasing their Ca^{2+} transient amplitudes ($P = 2.5 \times 10^{-12}$ and $P = 9.8 \times 10^{-9}$, respectively), RyR2-DKI transients were significantly smaller compared with WT cells ($P = 0.0002$; Fig. 3*E*). This was associated with a reduced SR Ca^{2+} content in RyR2-DKI myocytes in comparison to WT cells ($P = 0.0334$; Fig. 3*G*). Noticeably, Ca^{2+} decay time remained significantly faster in RyR2-DKI myocytes during Iso stimulation (Fig. 3*F*).

It has been shown that the time constant (τ) of the Ca^{2+} transient decay depends on both sarcoendoplasmic calcium ATPase (SERCA) activity and the amplitude of the Ca^{2+} signal itself (Bers & Berlin, 1995). To correct for differences in this feature, we selected pairs of triggered transients with similar amplitudes (±1% difference) for WT and RyR2-DKI and again observed a significant difference ($P = 1.7 \times 10^{-5}$). This enhanced SERCA activity is in agreement with western blotting, revealing a reduced phospholamban (PLB) expression (Fig. 4). The reduced PLB expression could be an adaptive change occurring in the DKI cardiomyocytes. Overall, Iso accelerated cytosolic Ca^{2+} removal in both cell types (WT, $P = 8.7 \times 10^{-26}$; RyR2-DKI, $P = 1.0 \times 10^{-23}$) compared with control conditions (Fig. 3*F*).

RyR2-DKI mouse cardiomyocytes exhibit an increased propensity for Ca^{2+} waves

To define whether the cellular characteristics of the RyR2-DKI myocytes exhibited above could restrain or enhance the arrhythmogenicity of RyR2-DKI myocytes, we determined the propensity of isolated myocytes to generate spontaneous Ca^{2+} waves (SCaW). In a first series of experiments, we measured the number of SCaWs and their latency after a conditioning train of field stimulation pulses (1 Hz). These are established indices of arrhythmogenicity at the cellular level (Fig. 3*A*). In control conditions, SCaWs (expressed as cells exhibiting one or more waves within an interval of 30 s) occurred more frequently in the RyR2-DKI myocytes compared with WT cells ($P = 0.0310$). In the presence of Iso, the incidence of SCaWs significantly increased in both WT and RyR2-DKI myocytes (Fig. 3*B*). The latency to the first SCaW decreased in the presence of Iso in cells from

Table 3. Electrogram analysis from wild-type and RyR2-double knock-in mice

Parameter	Units	WT ($N = 6$)	RyR2-DKI ($N = 5$)	*P*-value
Baseline				
Heart rate	beats per minute	476.49 ± 31.05	562.22 ± 15.85**	0.0003
P duration	milliseconds	6.78 ± 1.10	9.41 ± 1.24**	0.0048
PR interval	milliseconds	35.59 ± 2.52	37.09 ± 4.62	0.5105
QRS interval	milliseconds	10.21 ± 0.70	10.77 ± 3.27	0.7237
QTc	milliseconds	20.48 ± 1.36	32.20 ± 12.10	0.0960
Isoprenaline + caffeine				
Heart rate	beats per minute	531.57 ± 26.98	593.19 ± 3.96**	0.0023
P duration	milliseconds	6.82 ± 1.39	9.16 ± 0.87**	0.0098
PR interval	milliseconds	39.08 ± 3.86	43.34 ± 7.95	0.2735
QRS interval	milliseconds	10.88 ± 1.02	12.28 ± 2.22	0.1964
QTc	milliseconds	23.48 ± 3.51	25.41 ± 4.72	0.4544

Data are shown as the mean ± SD. Significant differences were assessed by Student's two-sample *t* test.
** $P < 0.01$ *vs*. WT.
Abbreviations: DKI, double knock-in; WT, wild type.

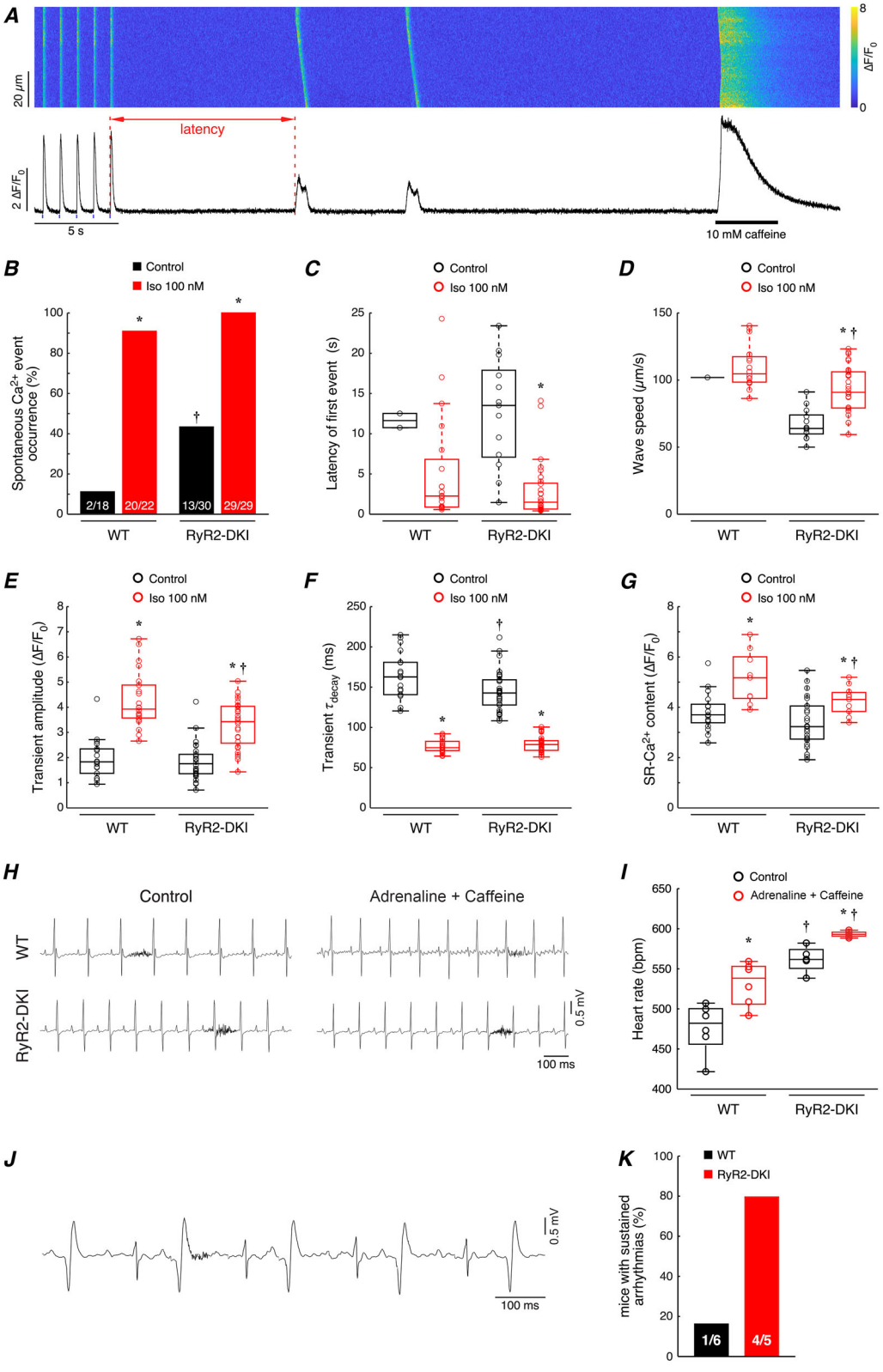

Figure 3. Analysis of parameters of arrhythmia
A, isolated ventricular myocytes were paced at 1 Hz for 30 s to study the propensity for pro-arrhythmic Ca^{2+} release. The confocal line-scan images and the fluorescence profile below show such an experiment, including

the last five triggered transients. These are followed by spontaneous Ca^{2+} releases (SCaW) and the application of caffeine (10 mmol/l) to determine sarcoplasmic reticulum (SR) Ca^{2+} content. The red double-headed arrow shows the latency to the first spontaneous Ca^{2+} release (SCaW) after the stimuli. *B*, the occurrence of SCaW (as a percentage of cells) was higher in RyR2-double knock-in (DKI) cells compared with wild type (WT) during control conditions. Isoprenaline (Iso; 100 nmol/l) increased the occurrence in both cell types. Significant differences were assessed by Fisher's exact test with Benjamini–Hochberg correction for pairwise comparisons. *C*, upon Iso treatment, the latency to the first SCaW was shorter in RyR2-DKI compared with control. *D*, Ca^{2+} wave speed was lower in the RyR2-DKI cells after Iso stimulation. *E*, Ca^{2+} transient amplitudes were smaller in the RyR2-DKI cells after Iso stimulation. *F*, the decay of the Ca^{2+} transients was significantly faster in RyR2-DKI in control conditions. Isoprenaline (red plots) accelerated the decay to a similar extent in WT and mutant myocytes. *G*, the SR Ca^{2+} content was significantly elevated after application of Iso in both types of cells. WT: $N = 6$, $n = 18–20$; RyR2-DKI: $N = 8$, $n = 29–30$ (*G*, WT: $N = 5–6$, $n = 9–17$; RyR2-DKI: $N = 6–8$, $n = 11–25$). Significant differences: $^{*}P < 0.05$ *vs*. control; $^{\dagger}P < 0.05$ *vs*. WT. *H*, representative electrocardiogram (ECG) traces in control conditions and during challenge protocol (adrenaline and caffeine). *I*, DKI mice exhibited a higher heart rate both in control conditions and under Iso and caffeine challenge. Two-way analysis of variance (ANOVA) with Tukey–Kramer *post hoc* test was used to assess significant differences among individual groups. *J*, a representative trace of ventricular bigeminy. *K*, incidence of sustained (>5 s) arrhythmias in WT and RyR2-DKI mice. Significant difference was assessed by Fisher's exact test. All measured ECG parameters are summarized in Table 3.

WT and mutant mice and was not remarkably different between groups ($P = 0.1589$; Fig. 3*C*). Finally, the speed of SCaWs was reduced in RyR2-DKI myocytes stimulated by Iso compared with that of WT myocytes ($P = 0.0041$; Fig. 3*D*). However, this subtle difference in wave speed was not present after normalizing for SR Ca^{2+} content (data not shown). These experiments suggest that the increase in RyR2-DKI activity is an intrinsic property of the mutant channel rather than being mediated by changes in SR Ca^{2+} load (Fig. 3*G*). In another set of experiments, we recorded surface ECGs from WT and RyR2-DKI mice in control conditions and under adrenaline and caffeine challenge to assess susceptibility to arrhythmias at the animal level (Fig. 3*H*). In baseline conditions, we confirmed the tachycardia observed in RyR2-DKI animals by echocardiography ($P = 3.0 \times 10^{-6}$). The challenge protocol caused a significant increase in the heart rate in both WT and RyR2-DKI mice (Fig. 3*I*). Notably, RyR2-DKI heartbeats remained faster than WT hearts ($P = 3.0 \times 10^{-6}$). Overall, RyR2-DKI animals displayed

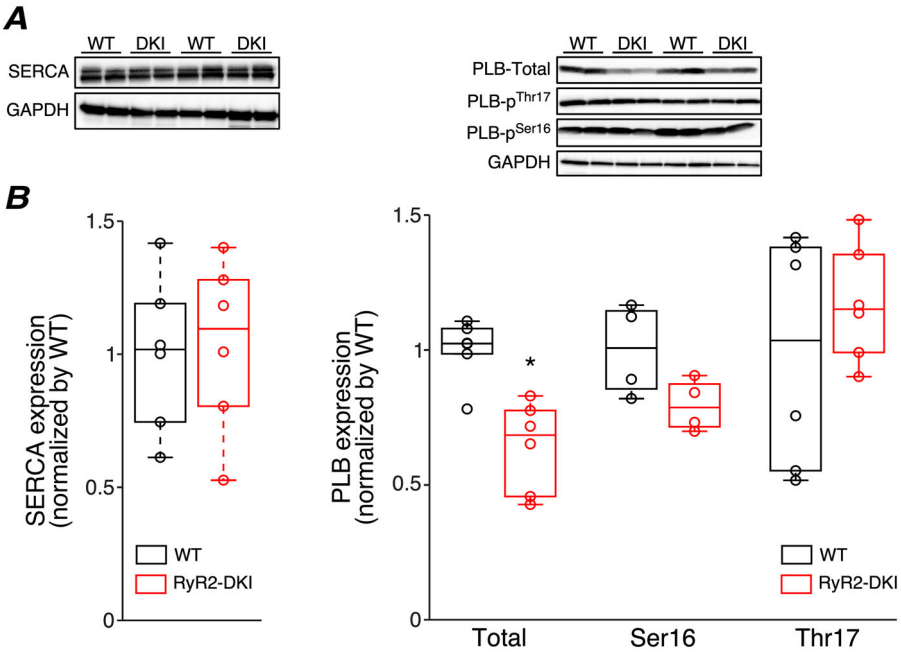

Figure 4. Increased sarcoendoplasmic calcium ATPase activity in the RyR2-double knock-in myocytes
A, representative western blots of total sarcoendoplasmic calcium ATPase (SERCA), total phospholamban (PLB) and phosphorylation of PLB-Ser16 and PLB-Thr17 in protein homogenates of wild-type (WT) and RyR2-double knock-in (DKI) hearts. *B*, quantification of SERCA and PLB expression and PLB phosphorylation. This shows that in mutant hearts the expression of PLB, the natural inhibitor of SERCA, is decreased ($P = 0.0015$, Student's two-sample *t* test), whereas its phosphorylation level is increased. This leads to higher SERCA activity in the RyR2-DKI hearts. $^{*}P < 0.05$ *vs*. WT.

increased susceptibility to arrhythmias over WT mice. RyR2-DKI mice typically presented with sustained (>5 s) ventricular bigeminy (Fig. 3*J* and *K*; $P = 0.0801$).

Ablation of two phosphorylation sites does not prevent cAMP-induced increases in CaSpF in permeabilized myocytes

Despite the lower SR Ca^{2+} load in RyR2-DKI cells, they displayed a higher occurrence of spontaneous Ca^{2+} waves. This could indicate a higher Ca^{2+} sensitivity of the RyR2-DKI channels, even in the absence of phosphorylation of these two sites. To examine the result of ablation of phospho-sites on RyR2 activity, we examined spontaneous Ca^{2+} sparks in intact cells (Fig. 5), then repeated the experiments in permeabilized myocytes (Fig. 6). In intact cells, RyR2 activity depends on its intracellular milieu, such as the cytosolic [Ca^{2+}], among other soluble constituents. Therefore, differences in activity measured between WT and mutant channels might reflect variations in cytosolic [Ca^{2+}] or other components between both types of cells that become equalized in permeabilized myocytes (Fig. 6*A*). Intact cells exhibited a small but significant increase in Ca^{2+} spark frequency in both control conditions ($P = 0.0219$) and in the presence of Iso ($P = 0.0219$) compared with that of WT myocytes (Fig. 5). In permeabilized myocytes, we detected no difference in Ca^{2+} sparks frequency (CaSpF) between WT and RyR2-DKI myocytes in control conditions (Fig. 6*B*). However, the acute dephosphorylation of RyR2 by PP1 significantly increased CaSpF in WT cells ($P = 7.2 \times 10^{-10}$), as we and others have reported before (Potenza et al., 2020; Terentyev et al., 2003), but did not change the CaSpF in RyR2-DKI cells ($P = 0.7111$). This suggests that acute dephosphorylation of Ser2808 and/or Ser2814 in the WT cells contributes significantly to the increase of CaSpF. In a second set of experiments, we applied cAMP to induce PKA-mediated phosphorylation of the available sites (Fig. 6*A* and *B*). As anticipated, cAMP significantly increased CaSpF of WT cells *vs*. both untreated conditions ($P = 7.5 \times 10^{-25}$) and PP1 treatment ($P = 0.0002$). Remarkably, in RyR2-DKI cells, where only Ser2030 remains as the most prominent PKA site, cAMP also increased CaSpF ($P = 2.4 \times 10^{-28}$ *vs*. control conditions) to similar levels as cAMP-treated WT myocytes ($P = 0.6736$).

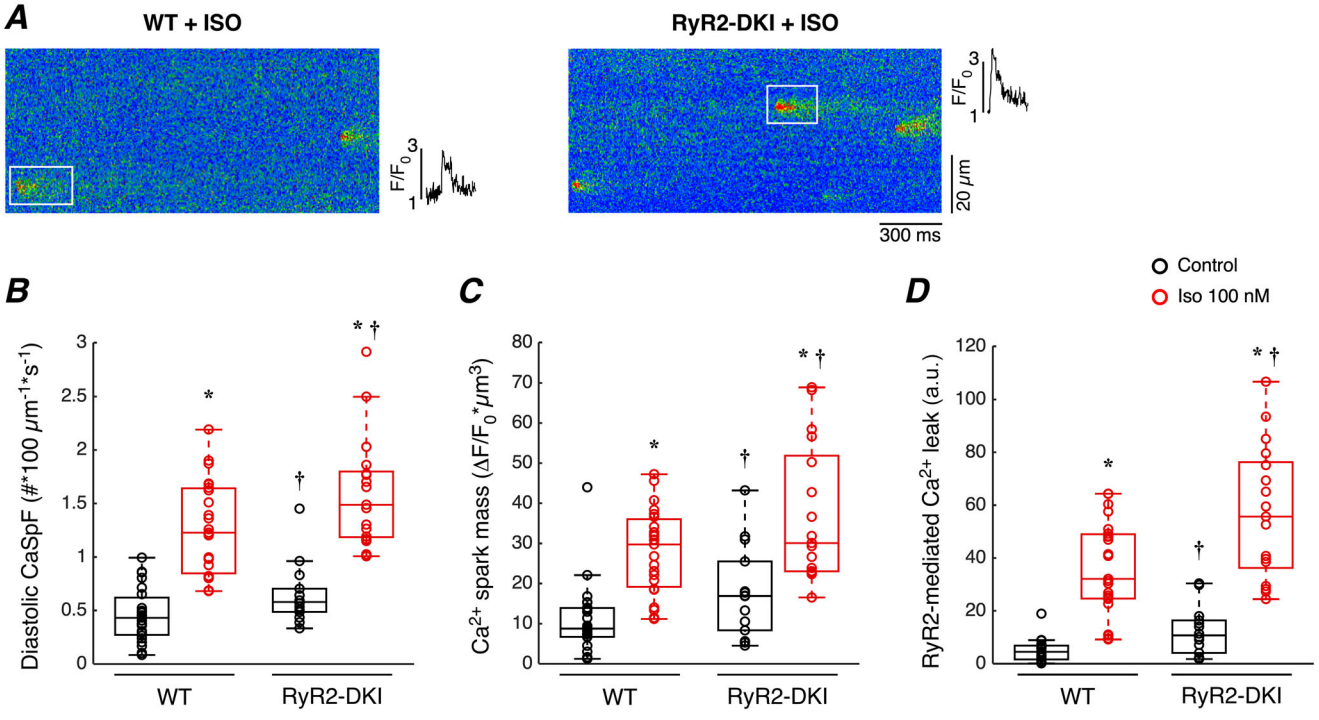

Figure 5. Calcium sparks in intact cells
Ablation of RyR2-Ser2808 and Ser2814 phosphorylation sites does not modify the frequency of the Ca^{2+} sparks, but results in the increase of sparks mass and RyR2-mediated Ca^{2+} leak both in control conditions and in the presence of isoprenaline (Iso). *A*, representative example of Ca^{2+} sparks recorded in wild-type (WT) and RyR2-double knock-in (DKI) myocytes. *B–D*, quantitative analysis of, respectively, Ca^{2+} spark frequency (CaSpF), Ca^{2+} spark mass and RyR2-mediated Ca^{2+} leak. For the WT group: $N = 4$ hearts and $n = 23$ myocytes; for the RyR2-DKI group: $N = 3$ hearts and $n = 14–17$ myocytes. Two-way analysis of variance (ANOVA) with Tukey–Kramer *post hoc* test was used to assess significant differences among individual groups. $^{*}P < 0.05$ *vs*. control; $^{\dagger}P < 0.05$ *vs*. WT.

This suggests that phosphorylation of Ser2030 is a major RyR2 functional site of the β-adrenergic response. This view is supported by previous findings in cardiomyocytes with an ablated RyR2-S2030 site. These experiments were carried out in conditions that kept the SERCA function constant by applying a PLB antibody fragment, thereby eliminating interfering changes in SERCA activity (Potenza et al., 2019). Nonetheless, given that PP1, in addition to PKA, alters the activity not only of RyR2s but also of SERCA via changes of PLB phosphorylation, we measured SR Ca^{2+} content to assess the influence of SR load on the differential CaSpF. Application of 20 mmol/l caffeine indicated similar SR Ca^{2+} content in WT and RyR2-DKI cells in control conditions ($P = 0.1861$; Fig. 6*C*), but lower SR Ca^{2+} loads in WT cells treated by PP1 ($P = 0.0240$). The SR Ca^{2+} content depletion in PP1-treated cells is likely to be the result of high RyR2-mediated Ca^{2+} leak. We also observed trends to higher SR Ca^{2+} content in the presence of cAMP compared with control conditions, both in WT ($P = 0.0414$) and RyR2-DKI ($P = 0.0490$), suggesting higher SERCA activity.

Threshold for spontaneous Ca^{2+} wave generation is lower in RyR2-DKI mice

A more pronounced propensity for Ca^{2+} waves in RyR2-DKI cells could result from an elevated intra-SR Ca^{2+} concentration or from an abnormally high sensitivity of the RyR2-DKI for cytosolic (or SR) Ca^{2+}. At rest, we did not observe a significant difference in SR Ca^{2+} load (Figs 3*G* and 6*C*). To define the Ca^{2+} wave initiation more precisely, we tried to elevate the SR Ca^{2+} load until Ca^{2+} waves started to appear. During these experiments, we recorded the intra-SR Ca^{2+} concentration with

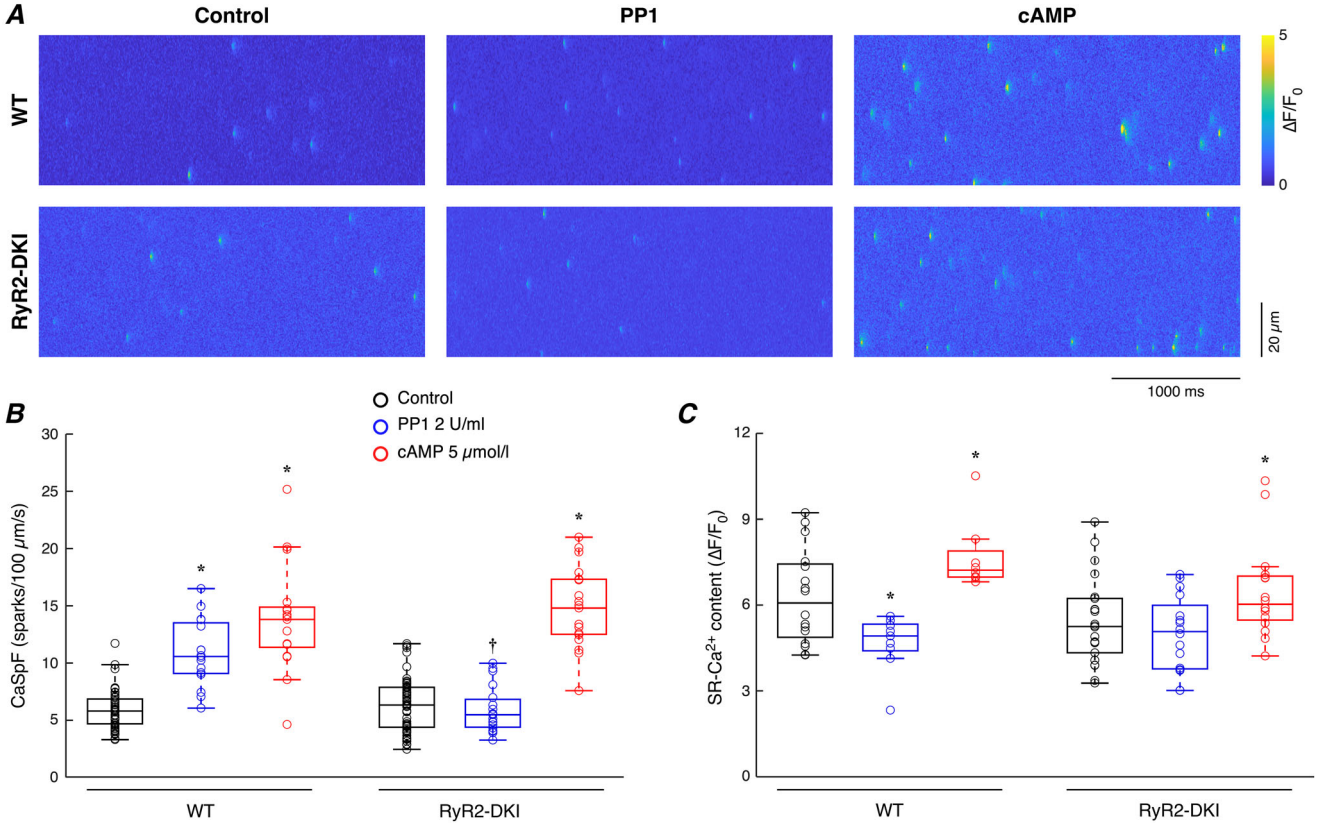

Figure 6. Acute dephosphorylation by protein phosphatase-1 increased Ca^{2+} spark frequency in wild-type but not in RyR2-double knock-in cells
A, confocal line-scan images of Ca^{2+} sparks recorded in permeabilized cells in control conditions, 1 min after exposure to protein phosphatase-1 (PP1; 2 U/ml) or 10 min after application of 5 μmol/l cyclic adenosine monophosphate (cAMP). *B*, basal Ca^{2+} spark frequency (CaSpF) was similar in both RyR2-double knock-in (DKI) and wild-type (WT) myocytes; PP1 increased the CaSpF in WT but failed to modify the spontaneous activity of mutant cells. cAMP elevated CaSpF in both types of cells. WT: $N = 5–8$, $n = 17–53$; RyR2-DKI: $N = 5–9$, $n = 19–61$. *C*, the amplitudes of the caffeine-induced Ca^{2+} transients were similar in control conditions between WT and RyR2-DKI. Only in WT myocytes was the increased CaSpF accompanied by partial depletion of the SR Ca^{2+} content. WT: $N = 4–6$, $n = 8–16$; RyR2-DKI: $N = 5–6$, $n = 16–22$. Significant differences: $^*P < 0.05$ *vs*. control and †$P < 0.05$ *vs*. WT.

Fluo-5N entrapped inside the SR (Fernandez-Tenorio & Niggli, 2016, 2018; Fig. 7*A*). When the intra-SR Ca^{2+} concentration in the permeabilized myocytes was elevated experimentally (by raising the cytosolic Ca^{2+} concentration to near 100 nmol/l), the threshold for Ca^{2+} wave generation (i.e. the SR Ca^{2+} level immediately before the initiation of a wave) was significantly lower in RyR2-DKI cells ($P = 0.0001$; Fig. 7*B*). In other words, the maximal SR Ca^{2+} concentration that could be reached before a Ca^{2+} wave occurred was lower in DKI cells. This lower intra-SR threshold for Ca^{2+} wave initiation suggests a higher sensitivity of RyR2-DKI channels for Ca^{2+}, which could underlie the elevated Ca^{2+} wave frequency. Please note that this finding is not at odds with the similar resting SR Ca^{2+} content in both cell types, because the conditions are very different in the two experiments.

RyR2-DKI cells harbour RyR2 channels with increased Ca^{2+} sensitivity

To quantify the RyR2 Ca^{2+} sensitivity of WT and RyR2-DKI channels *in situ*, we performed a Ca^{2+} spark recovery analysis. For this assay, a very low dose of ryanodine is applied to only lock a few (1–10) RyR2 channels per cell in a subconductance open state. Such ryanodine-modified RyR2s might induce self-repeating sparks from one release site (also known as a couplon) for a limited time (≤8 min; Poláková et al., 2015; Potenza et al., 2019). The delay for spark recovery is estimated from the median of spark-to-spark delay histograms. In validation experiments, we showed that pharmacological interventions increasing RyR2 sensitivity to Ca^{2+} (e.g. a low concentration of caffeine) shorten spark-to-spark delay times, whereas compounds reducing RyR2 sensitivity to Ca^{2+} (e.g. tetracaine) extend it (Poláková et al., 2015; Potenza et al., 2019). Based on such experiments, we expected RyR2-DKI cells to show shorter spark-to-spark delays in control conditions and in response to Iso, if these channels were indeed more Ca^{2+} sensitive. Thus, we measured the spark-to-spark delay (Fig. 8*A*) and the relative spark amplitudes (not shown) to investigate Ca^{2+} spark restitution. Consistent with the lower Ca^{2+} wave thresholds shown above, we observed a significantly shorter spark-to-spark delay median in control conditions in RyR2-DKI cells ($P = 0.0065$; Fig. 8*B* and *C*). Myocytes from both animal types responded to Iso with a significant shift of spark-to-spark medians towards shorter times in comparison to control conditions ($P = 5.6 \times 10^{-9}$ for WT and $P = 1.3 \times 10^{-15}$ for RyR2-DKI). We also found a significant difference in the presence of Iso between WT and mutant cells ($P = 3.6 \times 10^{-13}$).

Taken together, the spark recovery analysis supports the notion of higher RyR2 Ca^{2+} sensitivity in RyR2-DKI cells, leading to a left shift of the recovery probability distribution in control conditions. Both WT and RyR2-DKI were sensitive to Iso, which increases the Ca^{2+} sensitivity further, presumably owing to RyR2 phosphorylation.

Discussion

The hyperphosphorylation hypothesis

Previous investigations into RyR2 phosphorylation primarily used biochemical techniques (e.g. Takasago et al., 1991; Witcher et al., 1991). However, it was not until the emergence of the RyR2 'hyperphosphorylation' hypothesis, proposed based on a combination of functional and biochemical studies (Marx et al., 2000), that this topic gained widespread attention and sparked intense debate. In their groundbreaking study, they analysed the RyR2 macromolecular complex, encompassing FK506-binding protein (FKBP12.6, also known as Calstabin-2), PKA along with its anchoring protein mAKAP, and the protein phosphatases PP1 and PP2A. In hearts afflicted by heart failure in both patients and dogs, RyR2-Ser2808 exhibited pronounced phosphorylation, reaching a state of 'hyperphosphorylation'. Single-channel experiments conducted on RyR2s from patients with heart failure, reconstituted into lipid bilayers, indicated an elevated channel open probability and abnormally heightened sensitivity to Ca^{2+}. The postulation at that time was that Ser2808 hyperphosphorylation would induce RyR2 'leakiness' and result in the depletion of SR Ca^{2+}, thereby contributing to the dysfunction of Ca^{2+} signalling and weakened cardiac contractions.

In subsequent, often controversial studies, multiple details of the RyR2 hyperphosphorylation hypothesis were analysed by several groups. This included the identity and molecular function of the various phosphorylation sites on the channel (e.g. Ser2808, Ser2814 and Ser2030) and the consequences of their phosphorylation, both in the course of cardiac diseases and during normal regulatory events, such as acute β-adrenergic receptor stimulation. For these studies, several crucial tools have been developed, such as phospho-site specific antibodies (Huke & Bers, 2008) and transgenic mice with phospho-ablation or constitutive phosphorylation of these sites (for review, see Dobrev & Wehrens, 2014). Using these tools, RyR2 phosphorylation has been studied at all levels of physiological complexity, from molecular to cellular, to whole hearts to intact animals. At the cellular level, Ca^{2+} signalling was usually probed, often including the analysis of spontaneous Ca^{2+} waves and sparks during diastole. None of these previous studies used an animal model with dual ablation of the two most important phospho-sites in the 'phosphorylation hotspot' of RyR2, such as the DKI we used here. Based on the observation

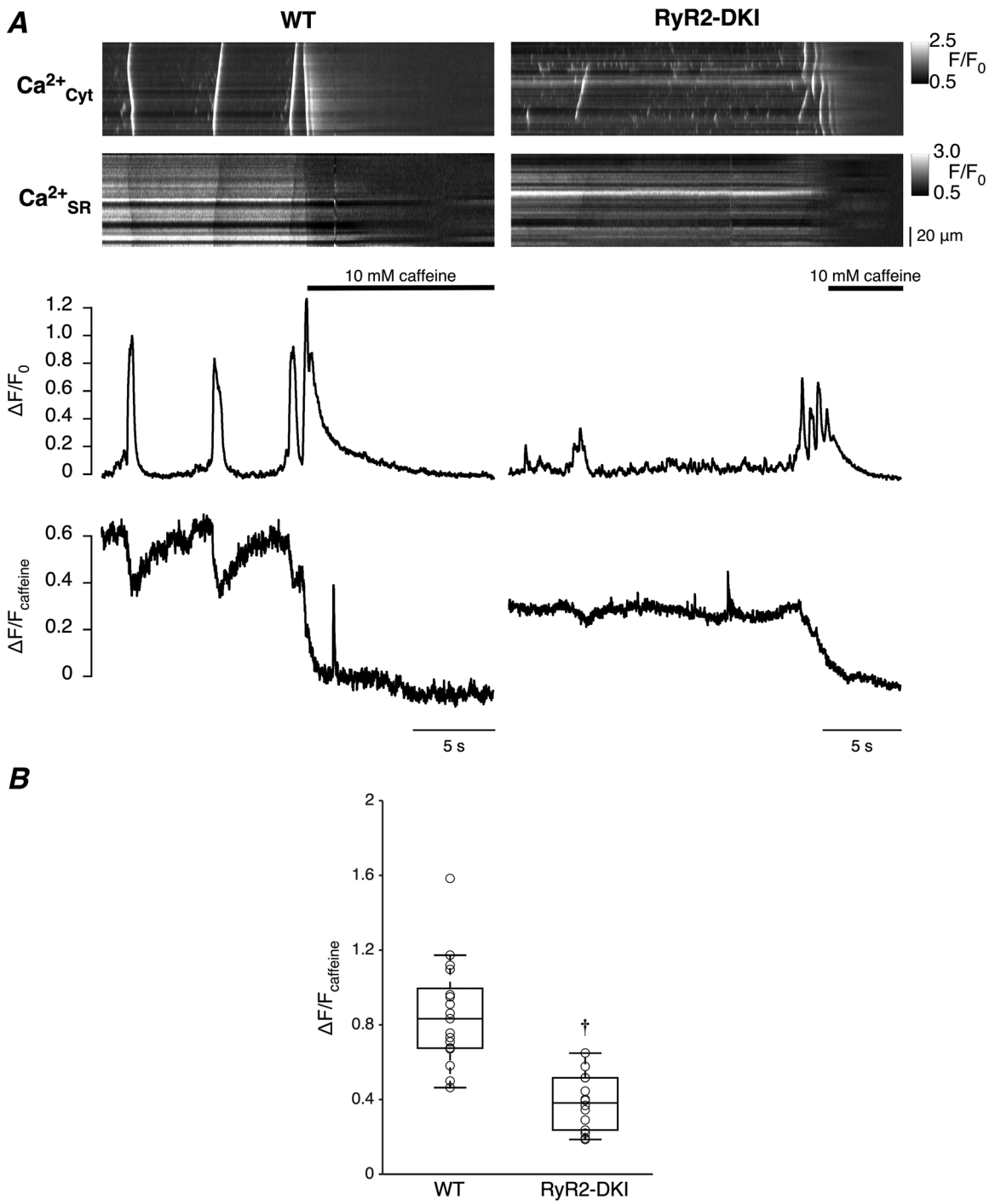

Figure 7. Estimates of intra-sarcoplasmic reticulum Ca^{2+} wave thresholds in wild-type and RyR2-double knock-in myocytes

A, representative line-scan images (upper panel) and respective traces (lower panel) of cytosolic (cyt) and sarcoplasmic reticulum (SR) luminal Ca^{2+} signals in permeabilized cardiomyocytes from wild-type (WT) and RyR2-double knock-in (DKI) mice. *B*, quantitative analysis of SR Ca^{2+} wave threshold in permeabilized cardiomyocytes with a cytoplasmic [Ca^{2+}] of 100 nmol/l. WT: N = 9, n = 17; RyR2-DKI: N = 6, n = 14. Significant differences: †$P < 0.05$ *vs*. WT.

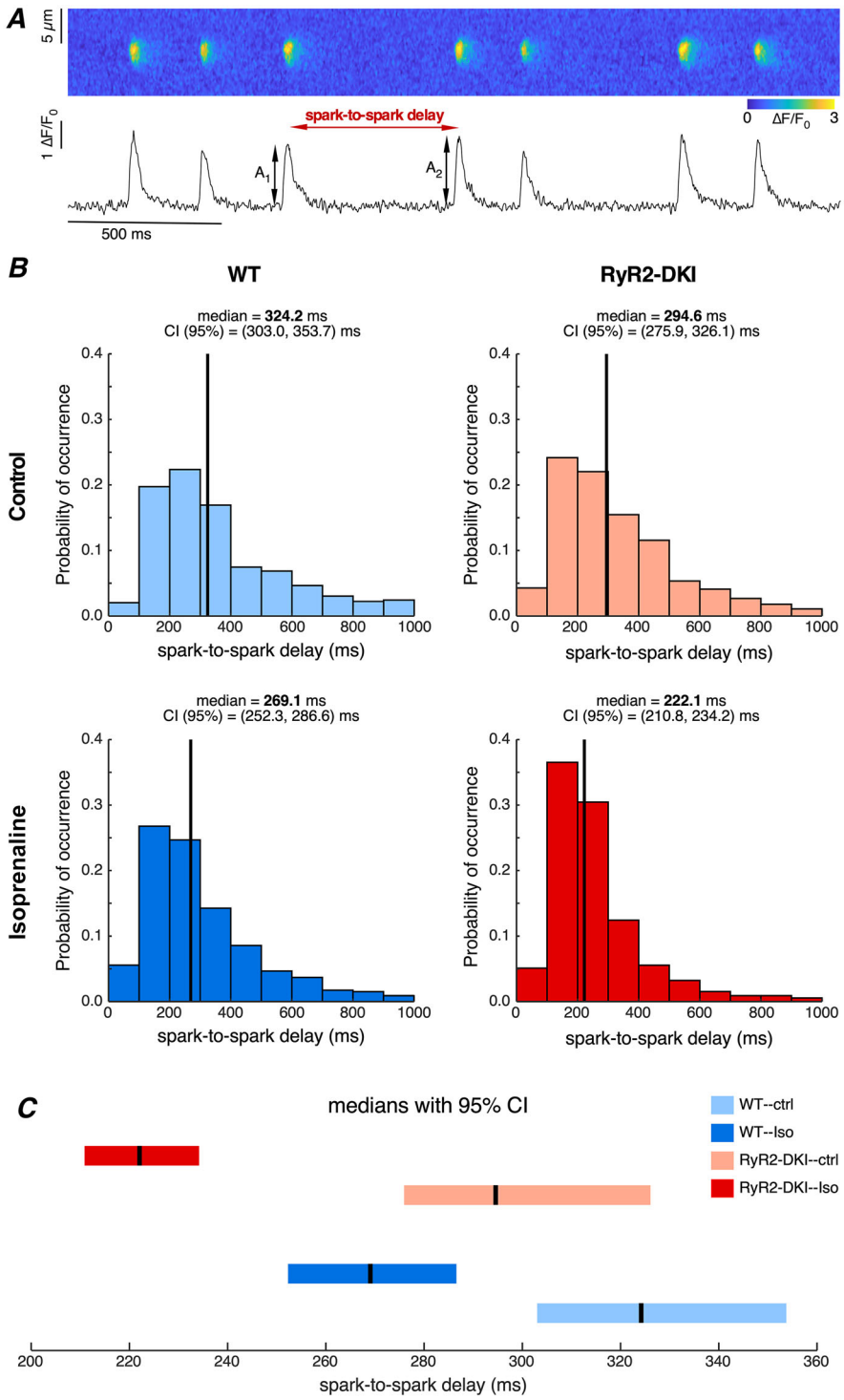

Figure 8. Spark recovery analysis indicates elevated Ca^{2+} sensitivity in RyR2-double knock-in cardiomyocytes
A, representative line-scan image in the presence of a very low concentration of ryanodine (50 nmol/l), which can induce repetitive sparks. *B*, histograms of delays of Ca^{2+} sparks in control conditions and in the presence of 100 nmol/l isoprenaline (Iso). Black vertical lines are medians of respective spark-to-spark delay distributions. *C*, summary and comparison of medians with 95% confidence intervals (CIs) of each individual group. Wild type (WT): control, N = 6, n = 25, 497 spark pairs; Iso, N = 6, n = 35, 1334 spark pairs. RyR2-double knock-in (DKI): control, N = 6, n = 18, 563 spark pairs; Iso, N = 6, n = 19, 1120 spark pairs. Individual groups were tested for significance using the Kruskal–Wallis test with Dunn–Sidak *post hoc* test.

that hyperphosphorylation of RyR2 channels increases their activity, one would expect that RyR2s from DKI mice would exhibit a normal or slightly reduced activity and a blunted response to β-adrenergic stimulation.

Role of RyR2 dephosphorylation

Given that, in the steady state, the extent of phosphorylation of the various sites reflects the balance of the activity of protein kinases and protein phosphatases, the consequences of dephosphorylation have also been studied, although in this case, the literature is not as extensive. A surprising observation was made in [^{3}H]ryanodine binding and lipid bilayer experiments with reconstituted RyR2s (Lokuta et al., 1995). Acute dephosphorylation was found to activate RyR2 channel function, rather than decrease it. Likewise, in isolated and permeabilized cardiomyocytes, perfusion of protein phosphatase (PP1 or PP2A) transiently increased CaSpF, subsequently depleting SR Ca^{2+} (Terentyev et al., 2003). The experiments above strongly suggested an activating role for RyR2 dephosphorylation, but given that externally applied phosphatases are of broad spectrum and do not target specific substrates, the identity of the affected RyR2 phospho-epitope(s) remained unknown. Fortunately, transgenic mice with selective ablation of specific RyR2 phospho-sites started to shed light on this question. Myocytes expressing the constitutively non-phosphorylatable Ser2808Ala site show only a subtle phenotype of cellular Ca^{2+} signalling and in limited experimental conditions (Ullrich et al., 2012). However, treatment of these cells with a phosphatase activator (or with PP1) failed to increase the CaSpF, which was readily observed in the WT cells. This suggests a role for acute Ser2808 dephosphorylation in WT cells in the activation of the RyR2 channel. This activation is only transient, because the SR subsequently loses Ca^{2+} (Potenza et al., 2020).

Animal models of RyR2 hyper- and dephosphorylation

Several transgenic mouse models have been engineered to examine the role of RyR2 phosphorylation. These animals harbour either a constitutively phosphorylation site (Ser2808Asp and Ser2814Asp) or a genetically ablated phosphorylation site (Ser2808Ala, Ser2814Ala and Ser2030Ala). [For a review of the functional consequences of these Ser2808 and Ser2814 site mutations see Dobrev & Wehrens (2014) and references therein.] Results from myocytes harbouring the Ser2030Ala mutation were described by Potenza et al. (2019). Generally, the phosphorylation-incompetent mutants have not shown an overt phenotype at the molecular, cellular or intact animal level during control conditions, despite the complete absence of phosphorylation at one given site (see Benkusky et al., 2007; Wehrens et al., 2006). In the case of Ser2808Ala and Ser2814Ala mice, both animals were somewhat protected from remodelling during heart failure in some, but not all, studies.

In the Ser2808Ala mice, some protection from the development of heart failure and remodelling after transverse aortic constriction or myocardial infarction has been reported (Wehrens et al., 2006), although this has not remained unchallenged (Alvarado et al., 2017; Benkusky et al., 2007; Zhang et al., 2012). Surprisingly, ECC regulation by β-adrenergic stimulation for the Ser2808Ala mouse was only subtly impaired at the cellular level (Ullrich et al., 2012) and unaltered at the whole heart and intact animal levels (Alvarado et al., 2017; Benkusky et al., 2007; Houser, 2010; Zhang et al., 2012). Cardiomyocytes from mice with the corresponding phosphomimetic mutation, Ser2808Asp, were reported to display increased RyR2 open probability, CaSpF and Ca^{2+} transient amplitudes in a few, but not all studies (Stange et al., 2003; Wehrens et al., 2006). These mice also purportedly developed spontaneous heart failure with age. In cardiomyocytes isolated from these animals, higher spontaneous CaSpF was observed (Dobrev & Wehrens, 2014).

Mice with combined dual ablation of Ser2808 and Ser2814 phospho-sites

Structural studies have revealed an intricate cross-talk mechanism between the phosphorylation sites Ser2808 and Ser2814, influencing each other's phosphorylation levels (Yuchi et al., 2012). Investigating the impact of simultaneous ablation of both Ser2808 and Ser2814 phosphorylation sites in an animal model is essential for gaining crucial insights into the collective role of these pivotal sites in regulating RyR2 channel function. Notably, in mice with dual ablation, where only the Ser2030 site remains functionally active among the typically assessed sites, a unique opportunity arises to dissect the specific contribution of Ser2030 phosphorylation independently from the phosphorylation of the other two relevant sites. Unexpectedly, these mice exhibited Ca^{2+} signalling and electrophysiological dysfunction even in control conditions. This unexpected outcome aligns with the concept that hypophosphorylation heightens the Ca^{2+} sensitivity of RyR2 channels, underscoring the intricate interplay of phosphorylation events in influencing channel behaviour.

Cellular and molecular features prevalent in the DKI cardiomyocytes

Experiments at the cellular level revealed functional remodelling of the DKI cardiac myocytes and their ECC,

but they occurred in the opposite direction to expected results. Although the L-type Ca^{2+} current amplitude was not altered, the Ca^{2+} transient amplitude was slightly larger in the DKI myocytes, resulting in a slightly higher ECC gain, particularly at positive membrane potentials. This is in line with the higher Ca^{2+} sensitivity of the RyR2, mentioned above, and the primary event leading to higher ECC gain.

Consistent with this notion, the propensity for spontaneous Ca^{2+} waves was higher in DKI cells, both in control conditions and in the presence of Iso. In addition, the latency (delay) to the first spontaneous Ca^{2+} wave after a train of field stimulations was shorter. Both parameters are considered cellular features of an arrhythmogenic phenotype. Indeed, bigeminy and other forms of arrhythmias were provoked more readily in DKI than in WT mice after injection of adrenaline and caffeine (Fig. 3).

The elementary Ca^{2+} signalling events, Ca^{2+} sparks, also provided several mechanistically interesting observations. In permeabilized WT cells, acute dephosphorylation by PP1 increased the CaSpF, as we reported before (Potenza et al., 2020). However, PP1 failed to increase CaSpF in DKI cells, arguing in favour of a crucial role for Ser2808 and/or Ser2814 phosphorylation in this parameter. Indeed, as detailed above, exposure to PP1 did not increase the CaSpF in RyR2-S2808A myocytes, in which only the Ser2808 site was selectively ablated (Potenza et al., 2020). Our results with the DKI cells also suggest that the Ser2367 phospho-site, which has recently been reported to increase RyR2 function upon dephosphorylation (Campbell et al., 2020), is not involved in the PP1-induced increase of CaSpF observed here.

What, then, explains the higher ECC gain and the higher propensity for Ca^{2+} waves in DKI cells? A plausible scenario includes an increased Ca^{2+} sensitivity of the RyR2s, for either cytosolic or luminal (intra-SR) Ca^{2+}, resulting in a lower SR Ca^{2+} release threshold. In the first series of experiments involving the recording of intra-SR Ca^{2+} concentrations, we found lowered Ca^{2+} wave thresholds in DKI cells when attempting to elevate intra-SR Ca^{2+} above control levels (Fig. 7). There was also a trend to lower SR Ca^{2+} content in control conditions and in the presence of Iso (Fig. 3*G*). Furthermore, Ca^{2+} spark recovery analysis revealed faster spark recovery in DKI cells, both in control conditions and in the presence of Iso (Fig. 8). Faster spark recovery is indicative of a higher Ca^{2+} sensitivity of the phosphomutant RyR2s. In addition, the shift in the presence of Iso in DKI cells strongly suggests that the Ser2030 site, which is intact in DKI cells, is sufficient for this type of regulation. This notion is also consistent with the complementary observation that the removal of the Ser2030 site limits the response to β-adrenergic receptor stimulation (Potenza et al., 2019).

A potential model to explain modulation of RyR2 by phosphorylation/dephosphorylation mechanisms

What purpose does it serve the RyR2 to be activated by dephosphorylation? The assumption that RyR2 dephosphorylation activates the RyR2 channel is based not only on the results presented here but also on the literature (Terentyev & Hamilton, 2016), and we hypothesize that the teleological meaning of this reaction is to increase Ca^{2+} release during parasympathetic stimulation (Ho et al., 2016). During resting periods, the sympathetic drive is minimal, as is the activity of PKA and CaMKII; if the efficiency of Ca^{2+} release was dependent only on these kinases, then modulation of cardiac performance at rest would be limited. An additional layer of RyR2 regulation could be gained by recruiting protein phosphatases for the control of Ca^{2+} release. In fact, we recently demonstrated that muscarinic stimulation of ventricular myocytes increases PKG activity, which might be responsible for the high basal levels of Ser2808 phosphorylation and might also disinhibit protein phosphatases that dephosphorylate RyR2 and increase the efficiency of Ca^{2+} release (Ho et al., 2016). Consistent with such a bimodal regulation, it has been shown that activation of PP1 by a peptide reduces SR Ca^{2+} leak in human heart failure (Fischer et al., 2018). During heart failure the RyR2 is known to be highly phosphorylated, and PP1 activation would be expected to move the balance of phosphorylation and dephosphorylation back towards the normal state and normal channel activity. Thus, both RyR2 phosphorylation and dephosphorylation might actively fine-tune Ca^{2+} release. Our hypothetical model is depicted in Fig. 9. In this model, phosphorylation activates the channel in a sigmoidal relationship, and dephosphorylation also activates the channel in a reciprocally inverted sigmoidal waveform. The dynamic range of RyR2 modulation by phosphorylation is thus an inverted bell-shaped curve resulting from the sum of both sigmoidal waveforms. Complete dephosphorylation (or 0% phosphorylation) brings about a maximal level of RyR2 activation, and the latter decreases as phosphorylation increases. When phosphorylation is high, dephosphorylation is correspondingly low, but the activation curve by phosphorylation dominates, resulting overall in higher RyR2 activity. This model might explain the concomitant modulation of RyR2 by phosphorylation and dephosphorylation mechanisms but does not identify the specific phospho-sites involved nor their hierarchical position in the general process.

Taken together, these findings demonstrate the fine balance between protein kinases and phosphatases that are crucial for cardiac function. Their interplay orchestrates a wide range of cellular electrophysiology and Ca^{2+} signalling functions that are mutually dependent on each other. Future strategies for therapeutical

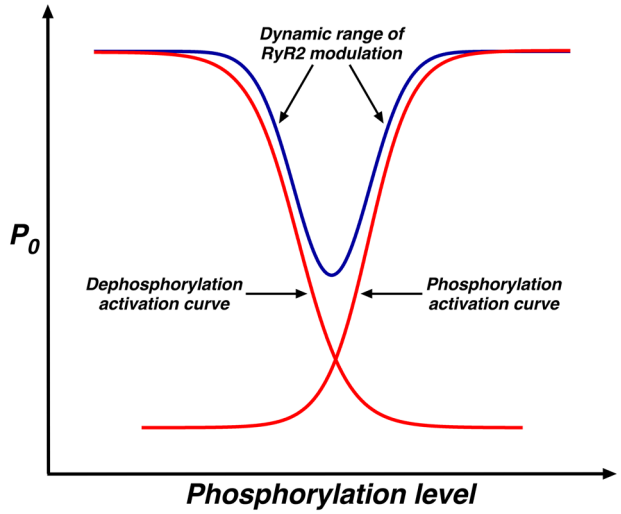

Figure 9. Proposed model for regulation of RyR2 activity by its degree of phosphorylation
Both protein kinases and protein phosphatases may increase RyR2 activity. The blue curve represents the dynamic range of bimodal regulation of RyR2 open probability (P_o) by dephosphorylation (left curve) and phosphorylation (right curve).

interventions targeting these signalling systems, either broadly or specifically, need to consider these various layers of complexity carefully.

References

Alvarado, F. J., Chen, X., & Valdivia, H. H. (2017). Ablation of the cardiac ryanodine receptor phospho-site Ser2808 does not alter the adrenergic response or the progression to heart failure in mice. *Journal of Molecular and Cellular Cardiology*, **103**, 40–47.

Bankhead, P., Scholfield, C. N., Curtis, T. M., & McGeown, J. G. (2011). Detecting Ca^{2+} sparks on stationary and varying baselines. *American Journal of Physiology-Cell Physiology*, **301**(3), C717–C728.

Benkusky, N. A., Weber, C. S., Scherman, J. A., Farrell, E. F., Hacker, T. A., John, M. C., Powers, P. A., & Valdivia, H. H. (2007). Intact beta-adrenergic response and unmodified progression toward heart failure in mice with genetic ablation of a major protein kinase A phosphorylation site in the cardiac ryanodine receptor. *Circulation Research*, **101**(8), 819–829.

Bers, D. M. (2002). Cardiac excitation-contraction coupling. *Nature*, **415**(6868), 198–205.

Bers, D. M., & Berlin, J. R. (1995). Kinetics of $[Ca]_i$ decline in cardiac myocytes depend on peak $[Ca]_i$. *The American Journal of Physiology*, **268**(1), C271–C277.

Camors, E., Loaiza, R., Alvarado, F., Powers, P., & Valdivia, H. H. (2012). Abstract 19322: Cardiac function and beta-adrenergic response in mice with genetic ablation of two major phosphorylation sites in the cardiac ryanodine receptor. *Circulation*, **126**, (Suppl_21), A19322.

Camors, E., Loaiza, R., Alvarado, F., Zhao, Y., Powers, P., & Valdivia, H. H. (2014). Preventing Ryr2-S2808 and Ryr2-S2814 phosphorylation does not alter the β-adrenergic response of mouse hearts. *Biophysical Journal*, **106**(2), 108a.

Camors, E., Mohler, P. J., Bers, D. M., & Despa, S. (2012). Ankyrin-B reduction enhances Ca spark-mediated SR Ca release promoting cardiac myocyte arrhythmic activity. *Journal of Molecular and Cellular Cardiology*, **52**(6), 1240–1248.

Camors, E. M., Roth, A. H., Alef, J. R., Sullivan, R. D., Johnson, J. N., Purevjav, E., & Towbin, J. A. (2022). Progressive reduction in right ventricular contractile function attributable to altered actin expression in an aging mouse model of arrhythmogenic cardiomyopathy. *Circulation*, **145**(21), 1609–1624.

Campbell, H. M., Quick, A. P., Abu-Taha, I., Chiang, D. Y., Kramm, C. F., Word, T. A., Brandenburg, S., Hulsurkar, M., Alsina, K. M., Liu, H. B., Martin, B., Uhlenkamp, D., Moore, O. M., Lahiri, S. K., Corradini, E., Kamler, M., Heck, A. J. R., Lehnart, S. E., Dobrev, D., & Wehrens, X. H. T. (2020). Loss of SPEG inhibitory phosphorylation of ryanodine receptor type-2 promotes atrial fibrillation. *Circulation*, **142**(12), 1159–1172.

Dobrev, D., & Wehrens, X. H. T. (2014). Role of RyR2 phosphorylation in heart failure and arrhythmias. *Circulation Research*, **114**(8), 1311–1319.

Fernandez-Tenorio, M., & Niggli, E. (2016). Real-time intra-store confocal Ca^{2+} imaging in isolated mouse cardiomyocytes. *Cell Calcium*, **60**(5), 331–340.

Fernandez-Tenorio, M., & Niggli, E. (2018). Stabilization of Ca^{2+} signaling in cardiac muscle by stimulation of SERCA. *Journal of Molecular and Cellular Cardiology*, **119**, 87–95.

Fischer, T. H., Eiringhaus, J., Dybkova, N., Saadatmand, A., Pabel, S., Weber, S., Wang, Y., Köhn, M., Tirilomis, T., Ljubojevic, S., Renner, A., Gummert, J., Maier, L. S., Hasenfuß, G., El-Armouche, A., & Sossalla, S. (2018). Activation of protein phosphatase 1 by a selective phosphatase disrupting peptide reduces sarcoplasmic reticulum Ca^{2+} leak in human heart failure. *European Journal of Heart Failure*, **20**(12), 1673–1685.

George, C. H. (2008). Sarcoplasmic reticulum Ca^{2+} leak in heart failure: Mere observation or functional relevance? *Cardiovascular Research*, **77**(2), 302–314.

Grundy, D. (2015). Principles and standards for reporting animal experiments in the Journal of Physiology and Experimental Physiology. *The Journal of Physiology*, **593**(12), 2547–2549.

Haji-Ghassemi, O., Yuchi, Z., & Van Petegem, F. (2019). The cardiac ryanodine receptor phosphorylation hotspot embraces Pka in a phosphorylation-dependent manner. *Molecular Cell*, **75**(1), 39–52. e4.

Ho, H.-T., Belevych, A. E., Liu, B., Bonilla, I. M., Radwański, P. B., Kubasov, I. V., Valdivia, H. H., Schober, K., Carnes, C. A., & Györke, S. (2016). Muscarinic stimulation facilitates sarcoplasmic reticulum Ca release by modulating ryanodine receptor 2 phosphorylation through protein kinase G and Ca/calmodulin-dependent protein kinase II. *Hypertension*, **68**(5), 1171–1178.

Hollingworth, S., Peet, J., Chandler, W. K., & Baylor, S. M. (2001). Calcium sparks in intact skeletal muscle fibers of the frog. *Journal of General Physiology*, **118**(6), 653–678.

Houser, S. R. (2010). Does protein kinase A–mediated phosphorylation of the cardiac ryanodine receptor play any role in adrenergic regulation of calcium handling in health and disease? *Circulation Research*, **106**(11), 1672–1674.

Huke, S., & Bers, D. M. (2008). Ryanodine receptor phosphorylation at Serine 2030, 2808 and 2814 in rat cardiomyocytes. *Biochemical and Biophysical Research Communications*, **376**(1), 80–85.

Loaiza, R., Benkusky, N. A., Powers, P. P., Hacker, T., Noujaim, S., Ackerman, M. J., Jalife, J., & Valdivia, H. H. (2013). Heterogeneity of ryanodine receptor dysfunction in a mouse model of catecholaminergic polymorphic ventricular tachycardia. *Circulation Research*, **112**(2), 298–308.

Lokuta, A. J., Rogers, T. B., Lederer, W. J., & Valdivia, H. H. (1995). Modulation of cardiac ryanodine receptors of swine and rabbit by a phosphorylation-dephosphorylation mechanism. *The Journal of Physiology*, **487**(3), 609–622.

Louch, W. E., Sheehan, K. A., & Wolska, B. M. (2011). Methods in cardiomyocyte isolation, culture, and gene transfer. *Journal of Molecular and Cellular Cardiology*, **51**(3), 288–298.

Marx, S. O., Reiken, S., Hisamatsu, Y., Jayaraman, T., Burkhoff, D., Rosemblit, N., & Marks, A. R. (2000). PKA phosphorylation dissociates FKBP12.6 from the calcium release channel (ryanodine receptor) defective regulation in failing hearts. *Cell*, **101**(4), 365–376.

Mondragón, R. R., Camors, E., Powers, P. P., & Valdivia, H. H. (2014). Ablation of major PKA and/or Camkii phosphorylation sites in the RyR2 channel differentially affects the susceptibility of mice to vagotonic atrial fibrillation. *Biophysical Journal*, **106**(2), 321a.

Niggli, E., Ullrich, N. D., Gutierrez, D., Kyrychenko, S., Poláková, E., & Shirokova, N. (2013). Posttranslational modifications of cardiac ryanodine receptors: Ca^{2+} signaling and EC-coupling. *Biochimica Et Biophysica Acta*, **1833**(4), 866–875.

Poláková, E., Illaste, A., Niggli, E., & Sobie, E. A. (2015). Maximal acceleration of Ca^{2+} release refractoriness by β-adrenergic stimulation requires dual activation of kinases PKA and CaMKII in mouse ventricular myocytes. *The Journal of Physiology*, **593**(6), 1495–1507.

Potenza, D. M., Janicek, R., Fernandez-Tenorio, M., Camors, E., Ramos-Mondragón, R., Valdivia, H. H., & Niggli, E. (2019). Phosphorylation of the ryanodine receptor 2 at serine 2030 is required for a complete β-adrenergic response. *Journal of General Physiology*, **151**(2), 131–145.

Potenza, D. M., Janicek, R., Fernandez-Tenorio, M., & Niggli, E. (2020). Activation of endogenous protein phosphatase 1 enhances the calcium sensitivity of the ryanodine receptor type 2 in murine ventricular cardiomyocytes. *The Journal of Physiology*, **598**(6), 1131–1150.

Sikkel, M. B., Francis, D. P., Howard, J., Gordon, F., Rowlands, C., Peters, N. S., Lyon, A. R., Harding, S. E., & MacLeod, K. T. (2017). Hierarchical statistical techniques are necessary to draw reliable conclusions from analysis of isolated cardiomyocyte studies. *Cardiovascular Research*, **113**(14), 1743–1752.

Sobie, E. A., Song, L., & Lederer, W. J. (2005). Local recovery of Ca^{2+} release in rat ventricular myocytes. *The Journal of Physiology*, **565**(2), 441–447.

Stange, M., Xu, L., Balshaw, D., Yamaguchi, N., & Meissner, G. (2003). Characterization of recombinant skeletal muscle (Ser-2843) and cardiac muscle (Ser-2809) ryanodine receptor phosphorylation mutants. *Journal of Biological Chemistry*, **278**(51), 51693–51702.

Takasago, T., Imagawa, T., Furukawa, K., Ogurusu, T., & Shigekawa, M. (1991). Regulation of the cardiac ryanodine receptor by protein kinase-dependent phosphorylation. *Journal of Biochemistry (Tokyo)*, **109**(1), 163–170.

Terentyev, D., & Hamilton, S. (2016). Regulation of sarcoplasmic reticulum Ca^{2+} release by serine-threonine phosphatases in the heart. *Journal of Molecular and Cellular Cardiology*, **101**, 156–164.

Terentyev, D., Viatchenko-Karpinski, S., Gyorke, I., Terentyeva, R., & Gyorke, S. (2003). Protein phosphatases decrease sarcoplasmic reticulum calcium content by stimulating calcium release in cardiac myocytes. *The Journal of Physiology*, **552**(1), 109–118.

Ullrich, N. D., Valdivia, H. H., & Niggli, E. (2012). PKA phosphorylation of cardiac ryanodine receptor modulates SR luminal Ca^{2+} sensitivity. *Journal of Molecular and Cellular Cardiology*, **53**(1), 33–42.

Valdivia, H. H. (2012). Ryanodine receptor phosphorylation and heart failure. *Circulation Research*, **110**(11), 1398–1402.

Wehrens, X. H. T., Lehnart, S. E., Reiken, S., Vest, J. A., Wronska, A., & Marks, A. R. (2006). Ryanodine receptor/calcium release channel PKA phosphorylation: A critical mediator of heart failure progression. *Proceedings of the National Academy of Sciences of the United States of America*, **103**(3), 511–518.

Wei, J., Guo, W., Wang, R., Paul Estillore, J., Belke, D., Chen, Y.-X., Vallmitjana, A., Benitez, R., Hove-Madsen, L., & Chen, S. R. W. (2023). Ryr2 serine-2030 Pka site governs Ca^{2+} release termination and Ca^{2+} alternans. *Circulation Research*, **132**(2), e59–e77.

Witcher, D. R., Kovacs, R. J., Schulman, H., Cefali, D. C., & Jones, L. R. (1991). Unique phosphorylation site on the cardiac ryanodine receptor regulates calcium channel activity. *Journal of Biological Chemistry*, **266**(17), 11144–11152.

Xiao, B., Jiang, M. T., Zhao, M., Yang, D., Sutherland, C., Lai, F. A., Walsh, M. P., Warltier, D. C., Cheng, H., & Chen, S. R. W. (2005). Characterization of a novel PKA phosphorylation site, serine-2030, reveals no PKA hyper-phosphorylation of the cardiac ryanodine receptor in canine heart failure. *Circulation Research*, **96**(8), 847–855.

Yuchi, Z., Lau, K., & Van Petegem, F. (2012). Disease mutations in the ryanodine receptor central region: Crystal structures of a phosphorylation hot spot domain. *Structure (London, England: 1993)*, **20**(7), 1201–1211.

Zhang, H., Makarewich, C. A., Kubo, H., Wang, W., Duran, J. M., Li, Y., Berretta, R. M., Koch, W. J., Chen, X., Gao, E., Valdivia, H. H., & Houser, S. R. (2012). Hyper-phosphorylation of the cardiac ryanodine receptor at serine 2808 is not involved in cardiac dysfunction after myocardial infarction. *Circulation Research*, **110**(6), 831–840.

Zhao, Y.-T., Valdivia, C. R., Gurrola, G. B., Powers, P. P., Willis, B. C., Moss, R. L., Jalife, J., & Valdivia, H. H. (2015). Arrhythmogenesis in a catecholaminergic polymorphic ventricular tachycardia mutation that depresses ryanodine receptor function. *Proceedings of the National Academy of Sciences of the United States of America*, **112**(13), E1669–E1677.

Zheng, J., Dooge, H. C., Pérez-Hernández, M., Zhao, Y.-T., Chen, X., Hernandez, J. J., Valdivia, C. R., Palomeque, J., Rothenberg, E., Delmar, M., Valdivia, H. H., & Alvarado, F. J. (2022). Preserved cardiac performance and adrenergic response in a rabbit model with decreased ryanodine receptor 2 expression. *Journal of Molecular and Cellular Cardiology*, **167**, 118–128.

Additional information

Data availability statement

Data used for the analysis will be made available through the public data repository Zenodo.org (DOI: https://doi.org/10.5281/zenodo.10282554).

Competing interests

The authors declare that they have no competing interests.

Author contributions

The study was conceived and designed by R.J., E.M.C., D.M.P., M.F.T., F.J.A., M.E., H.H.V., E.N. Acquisition and analysis of data for the work: R.J., E.M.C., D.M.P., M.F.T., Y.Z., H.D., R.L., F.J.A. Drafting the work and revising it critically for important intellectual content: R.J., E.M.C., D.M.P., M.F.T, F.J.A., M.E., H.H.V., E.N. All authors have approved the final version of the manuscript and agree to be accountable for all aspects of the work. All persons designated as authors qualify for authorship, and all those who qualify for authorship are listed.

Funding

This project was supported by the Swiss National Science Foundation (SNSF grants 31003A-179325 and 310030-156375 to E.N., 310030-185211 to M.E.), the National Institutes of Health grants R01HL055438 and R01HL170144 (to H.H.V.), R01HL161070 (to F.J.A.) and R01HL167195 (to H.H.V. and F.J.A.) and Novartis Research Foundation to M.E.

Acknowledgements

We would like to thank Marianne Courtehoux, Michael Känzig and Fang Liu for expert technical help.

Open access funding provided by Universitat Bern.

Keywords

Ca^{2+}-induced Ca^{2+} release, cardiac muscle, dephosphorylation, excitation–contraction coupling, protein phosphatase, ryanodine receptor 2

Supporting information

Additional supporting information can be found online in the Supporting Information section at the end of the HTML view of the article. Supporting information files available:

Peer Review History